JCI The Journal of Clinical Investigation

MEF2D sustains activation of effector Foxp3^{+} Tregs during transplant survival and anticancer immunity

Eros Di Giorgio, … , Ulf H. Beier, Wayne W. Hancock

J Clin Invest. 2020;130(12):6242-6260. https://doi.org/10.1172/JCI135486.

Research Article | Immunology | Oncology

Graphical abstract

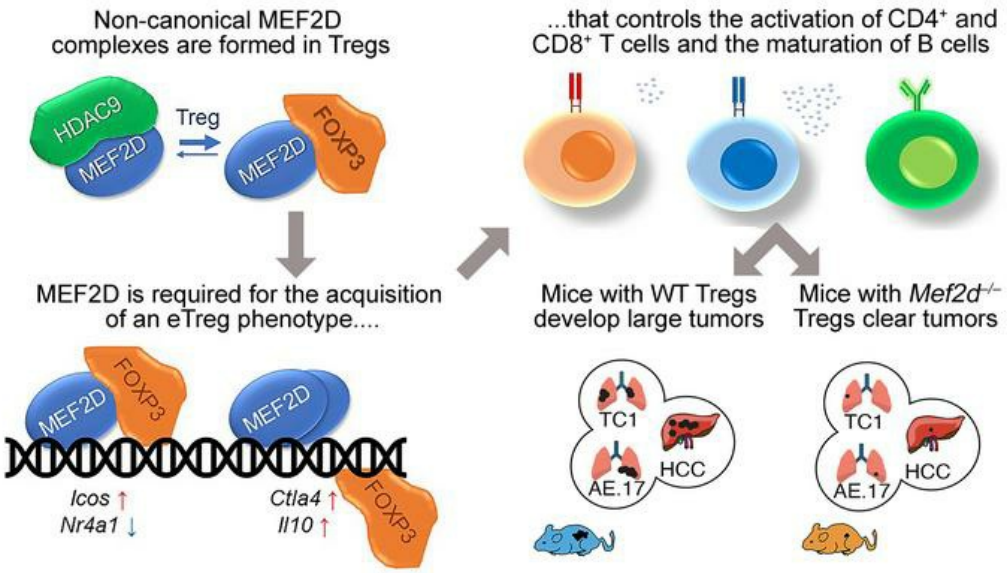

MEF2D sustains activation of effector Foxp3$^+$ Tregs during transplant survival and anticancer immunity

Eros Di Giorgio,[1,2] Liqing Wang,[1] Yan Xiong,[1,3] Tatiana Akimova,[1] Lanette M. Christensen,[1] Rongxiang Han,[1] Arabinda Samanta,[1] Matteo Trevisanut,[1,2] Tricia R. Bhatti,[4] Ulf H. Beier,[5] and Wayne W. Hancock[1]

[1]Division of Transplant Immunology, Department of Pathology and Laboratory Medicine, Children's Hospital of Philadelphia and Perelman School of Medicine, University of Pennsylvania, Philadelphia, Pennsylvania, USA. [2]Department of Medicine, Università degli Studi di Udine, Udine, Italy. [3]Institute of Hepatobiliary Diseases of Wuhan University, Transplant Centre of Wuhan University, Zhongnan Hospital of Wuhan University, Wuhan University, Wuhan, China. [4]Division of Anatomical Pathology, Department of Pathology and Laboratory Medicine, Children's Hospital of Philadelphia and Perelman School of Medicine, University of Pennsylvania, Philadelphia, Pennsylvania, USA. [5]Division of Nephrology, Department of Pediatrics, Children's Hospital of Philadelphia and Perelman School of Medicine, University of Pennsylvania, Philadelphia, Pennsylvania, USA.

The transcription factor MEF2D is important in the regulation of differentiation and adaptive responses in many cell types. We found that among T cells, MEF2D gained new functions in Foxp3$^+$ T regulatory (Treg) cells due to its interactions with the transcription factor Foxp3 and its release from canonical partners, like histone/protein deacetylases. Though not necessary for the generation and maintenance of Tregs, MEF2D was required for the expression of IL-10, CTLA4, and Icos, and for the acquisition of an effector Treg phenotype. At these loci, MEF2D acted both synergistically and additively to Foxp3, and downstream of Blimp1. Mice with the conditional deletion in Tregs of the gene encoding MEF2D were unable to maintain long-term allograft survival despite costimulation blockade, had enhanced antitumor immunity in syngeneic models, but displayed only minor evidence of autoimmunity when maintained under normal conditions. The role played by MEF2D in sustaining effector Foxp3$^+$ Treg functions without abrogating their basal actions suggests its suitability for drug discovery efforts in cancer therapy.

Introduction

The roles played by T regulatory (Treg) cells in the maintenance of immune homeostasis are well established (1). By restricting T cell functions, Tregs restrain the onset of autoimmunity but also dampen anticancer immunity (2). The transcription factor Foxp3 is required but not sufficient to sustain the immunosuppressive properties of Tregs (3). Pioneer factors (4–6) pave the way for Foxp3 expression in concert with a large number of epigenetic regulators that modulate its activities (7–13).

Besides the assembly and regulation of large multiprotein complexes containing Foxp3, the execution and the sustainment of the Treg program requires the activation of other transcription factors that act as genetic modulators (14). The action of these transcription factors may be supportive to Foxp3, like Thpok (15), or may be independent and additive or subtractive to Foxp3 (14). In particular, the coexpression of master transcription factors along with Foxp3 marks some Treg subsets, e.g., colonic Tregs coexpressing RORγt and Foxp3 (16, 17), or follicular Tregs (Tfr) coexpressing Bcl6 and Foxp3 (18, 19). In these various Treg subsets, the sum of the genetic responses triggered by the simultaneous activation of multiple master factors lets them acquire functional nuances more suited to their location (20). In other cases, in response to certain stimuli the activation of transcription factors such as Blimp1 and Irf4 can synergize with Foxp3 and trigger a reinforced Treg program that characterizes so-called effector Tregs (eTregs) (21).

MEF2D belongs to the myocyte enhancer factor-2 (MEF2) family of transcription factors (22). The weak intrinsic transcriptional activity of MEF2D can be potentiated by the binding of coactivators, like p300 (23), or completely blocked or even converted into transcriptional repression by the actions of corepressors, like class IIa histone/protein deacetylases (Hdacs) (24). The great plasticity of MEF2 transcription factors allows the precise modulation of differentiative and adaptive responses (22). Moreover, their binding to tissue-specific cofactors allows MEF2 transcription factors to play key roles in supervising the transcriptional program that underlies heterogeneous processes such as muscle differentiation, ossification, cardiac hypertrophy, synaptogenesis, and lymphoid commitment (22).

MEF2D is known to be highly expressed in T cells (25). In activated T cells, MEF2D sustains the production of IL-2 (26, 27), IL-4, and IFN-γ (28), as a consequence of its release from class IIa Hdacs and Cabin1 inhibition (26–28). In the thymus, MEF2D regulates the negative selection of double-positive T cells by promoting the transcription of Nurr77 in an Hdac7-dependent manner (29). Moreover, the inhibition or the knockout of the MEF2 repressor Hdac9 increases the suppressive properties of Treg cells (30), at least in part by sustaining the metabolic switch to OXPHOS that is characteristic of these CD4$^+$Foxp3$^+$ cells (31). Conversely, the

Authorship note: EDG and LW contributed equally to this work.
Conflict of interest: The authors have declared that no conflict of interest exists.

Submitted: December 12, 2019; **Accepted:** August 6, 2020; **Published:** October 26, 2020.
Reference information: *J Clin Invest*. 2020;130(12):6242–6260.
https://doi.org/10.1172/JCI135486.

expression of a gain-of-function mutant of Hdac7 decreases the proportion of Tregs (32).

In this study, we analyzed the still unexplored roles of MEF2D in CD4$^+$Foxp3$^+$ Treg cells. We focused on MEF2D because it was by far the most highly expressed member of the MEF2 family of paralogs in both human and murine Tregs. We found that MEF2D interacts with Foxp3 and modulates its activities, but also exerts Foxp3-independent functions required for Treg fitness. In addition, depletion of MEF2D in Treg cells dampens the Foxp3 program, especially in supraphysiological conditions that stimulate inflammation, such as transplantation and cancer.

Results

Foxp3 controls the expression and alternative splicing of MEF2D. Human and murine CD4$^+$Foxp3$^+$ Tregs express high levels of MEF2D (Supplemental Figure 1, A and B, respectively; supplemental material available online with this article; https://doi.org/10.1172/JCI135486DS1), and Foxp3 binds to the *Mef2d* promoter in both human and murine Tregs (Supplemental Figure 1, C and D). Comparison of MEF2D mRNA and protein levels in T effector (Teff) and Treg cells from C57BL/6 mice shows approximately 2-fold more *Mef2d* in Treg cells (Figure 1, A and B). We noticed that the genomic region of *Mef2d* encoding the 2 alternative third exons (3α1 and 3α2, Figure 1C) has chromatin features (H3K27ac and H3K36me3) typical of their active splicing in human Tregs but not in Teff cells (Supplemental Figure 1E). Moreover, the α2 isoform of MEF2D is reported to be expressed not only in muscle cells and neurons, but also in the spleen (33). We confirmed that the slight increase in MEF2D levels observed in freshly isolated Tregs with respect to Teffs is at least in part due to the expression of the α2 isoform (Figure 1, D and E). This increase was stronger after 24 hours of stimulation with anti-CD3/anti-CD28 antibodies and IL-2 (Figure 1, D and E). In these conditions, a slight increase in the α1 transcript can also be observed (Figure 1D), probably as a consequence of higher transcriptional activity on the *Mef2d* promoter. However, differently from the α2 isoform, the protein levels of the α1 isoform were not increased after stimulation, likely as a consequence of the increased instability of this isoform that selectively undergoes proteasomal degradation (34). Foxp3 is necessary to trigger the expression of the α2 isoform since suppression of Foxp3 led to significant decreases in the mRNA and protein levels of the α2 isoform, while the α1 isoform was minimally affected (Figure 1, G–I). Moreover, prolonged stimulation for 60 hours with anti-CD3/anti-CD28 mAbs and IL-2 stimulated the transcription of both the α1 and α2 isoforms of MEF2D, though with different magnitudes (2 and 10 times, respectively) (Figure 1F). While the α1 isoform is reported to be widespread though all the tissues of the body, the α2 isoform has a restricted pattern of expression and influences differentiative (35, 36) and adaptative (37, 38) responses. Moreover, compared with the α1 isoform, the α2 isoform encodes a stronger transcription factor since it lacks the phosphorylation sites of PKA (36) and CDK4/6 (34) that mediate the inhibition or proteasomal degradation of MEF2D. We conclude that, in contrast to Teffs, Tregs are characterized by an increase in MEF2D levels and by the Foxp3-dependent expression of the α2 isoform of MEF2D.

Foxp3 influences the assembly of MEF2D complexes. Foxp3 forms multiprotein complexes containing different transcription factors (7, 39). To test whether MEF2D can be part of such complexes, we transfected HEK293T cells with the α1 isoform of MEF2D, p300, and Foxp3. As shown in Figure 1J, MEF2D was stabilized by the coexpression of p300, and it interacted with both p300 and Foxp3, while the coexpression of Foxp3 and p300 did not perturb their binding to MEF2D (Figure 1J). Foxp3 did not bind to the DNA binding domain of MEF2D, as the deletion of this region did not abolish their interaction (Figure 1K). Moreover, the immunoprecipitation (IP) of MEF2D led to co-IP of Foxp3 in both freshly isolated and stimulated Tregs (Figure 1L). MEF2D bound strongly to p300 both in Teffs and in Tregs (resting or activated), while its binding to Hdac3 and Hdac9 was decreased in Tregs compared with Teffs, and respectively severely impaired or abolished after stimulation (Figure 1L). This could also be due to the decreased protein levels of Hdac3 and Hdac9 observed after stimulation (Figure 1L). We hypothesized that the different stoichiometry of MEF2D complexes between Tregs and Teffs could be due to the increased α2 isoform observed in Foxp3$^+$ cells. This was the case, because in freshly purified Tregs only the α1 isoform of MEF2D interacted strongly with Hdac9, whereas Foxp3 preferentially interacted with the α2 isoform (Figure 1M). To further assess these interactions, we transfected HEK293T cells with the 2 isoforms of MEF2D plus Foxp3 or Hdac9, and we pulled down MEF2D with isoform-specific Abs (Figure 1N). We found that the α2 isoform of MEF2D interacted strongly with Foxp3 and weakly with Hdac9 compared with the α1 isoform (Figure 1N). In reciprocal studies, IP of Foxp3 led to co-IP of MEF2D (Figure 1O). We conclude that in Tregs, different complexes assemble on MEF2D isoforms in response to Foxp3 expression and exogenous stimulation.

Characterization of Tregs deficient for MEF2D. Two different complexes assemble on MEF2D in Tregs. Only one, mainly associated with the α1 isoform, contains strong repressors like Hdac9. We hypothesized that both of these complexes are required to maintain Treg immune suppressive properties; the first, the repressive one, might be required to switch off some MEF2D genetic programs, while the second one might sustain and promote the expression of Treg-specific genes. To prove this concept, we conditionally deleted *Mef2d* in Foxp3$^+$ Treg cells by crossing *Mef2d*$^{fl/fl}$ mice (40) and *Foxp3*$^{YFP\text{-}Cre}$ mice. The KO allele encodes for a protein with an in-frame deletion of the second exon that is involved in DNA binding and dimerization, leading to the complete loss of function of the protein (40, 41). *Mef2d*$^{fl/fl}$ *Foxp3*$^{YFP\text{-}Cre}$ (hereafter *Mef2d*$^{-/-}$) mice were born at expected Mendelian ratios and appeared to develop normally over 1 year of monitoring. However, tissues from *Mef2d*$^{-/-}$ mice were characterized by the presence of mild mononuclear cell infiltrates in the lung and liver upon histologic examination, while they did not show any defects in colon, skin, pancreas, thymus, or other tissues (Supplemental Figure 2). Gene deletion was assessed by purifying Treg cells from WT and *Mef2d*$^{-/-}$ mice and confirming MEF2D deletion by immunoblot (Figure 2A). Moreover, as expected, the depletion of a functional MEF2D protein impaired the expression of the MEF2D target gene, *Hdac9* (Figure 2A). We further characterized the *Mef2d*$^{-/-}$ mice by harvesting secondary lymphoid tissues and assessing their cell populations by flow cytometry. *Mef2d*$^{-/-}$ mice were characterized by increased proportions of CD4$^+$Foxp3$^+$ Tregs within lymph nodes, spleen, and thymus (Figure 2, B and C), and by increased proportions of splenic CD4$^+$CD69$^+$

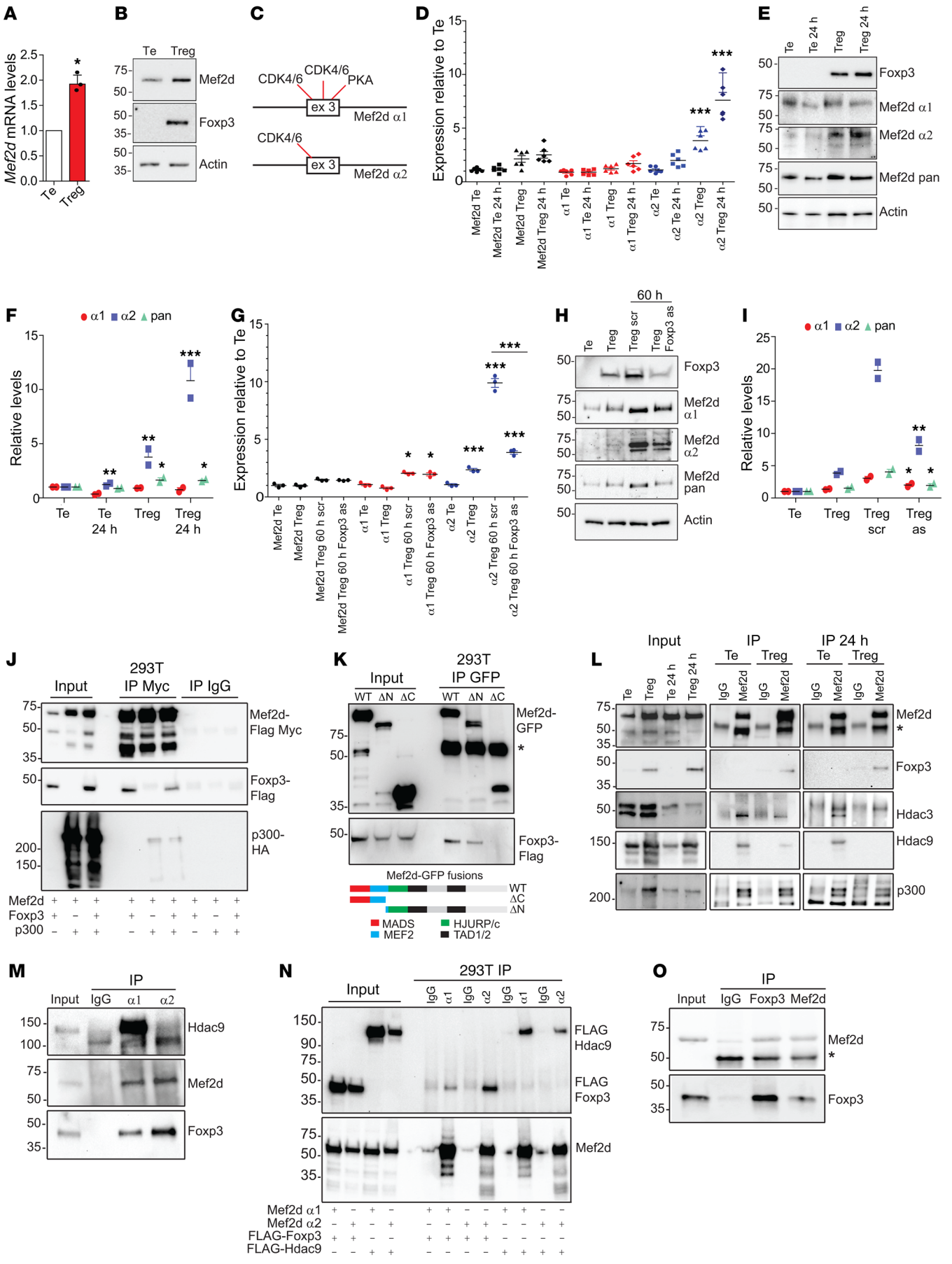
A
Mef2d mRNA levels
Te
Treg
B
Te
Treg
Mef2d
Foxp3
Actin
C
CDK4/6
CDK4/6
PKA
ex 3
Mef2d α1
CDK4/6
ex 3
Mef2d α2
D
Expression relative to Te
Mef2d Te
Mef2d Te 24 h
Mef2d Treg
Mef2d Treg 24 h
α1 Te
α1 Te 24 h
α1 Treg
α1 Treg 24 h
α2 Te
α2 Te 24 h
α2 Treg
α2 Treg 24 h
E
Te
Te 24 h
Treg
Treg 24 h
Foxp3
Mef2d α1
Mef2d α2
Mef2d pan
Actin
F
α1 α2 pan
Relative levels
Te
Te 24 h
Treg
Treg 24 h
G
Expression relative to Te
Mef2d Te
Mef2d Treg
Mef2d Treg 60 h scr
Mef2d Treg 60 h Foxp3 as
α1 Te
α1 Treg
α1 Treg 60 h scr
α1 Treg 60 h Foxp3 as
α2 Te
α2 Treg
α2 Treg 60 h scr
α2 Treg 60 h Foxp3 as
H
60 h
Te
Treg
Treg scr
Treg Foxp3 as
Foxp3
Mef2d α1
Mef2d α2
Mef2d pan
Actin
I
α1 α2 pan
Relative levels
Te
Treg
Treg scr
Treg as
J
293T
Input
IP Myc
IP IgG
Mef2d-Flag Myc
Foxp3-Flag
p300-HA
Mef2d
Foxp3
p300
K
293T
Input
IP GFP
WT ΔN ΔC
Mef2d-GFP
Foxp3-Flag
Mef2d-GFP fusions
WT
ΔC
ΔN
MADS
MEF2
HJURP/c
TAD1/2
L
Input
IP
IP 24 h
Te
Treg
Te 24 h
Treg 24 h
IgG
Mef2d
Foxp3
Hdac3
Hdac9
p300
M
IP
Input
IgG
α1
α2
Hdac9
Mef2d
Foxp3
N
293T IP
Input
IgG
α1
α2
FLAG Hdac9
FLAG Foxp3
Mef2d
Mef2d α1
Mef2d α2
FLAG-Foxp3
FLAG-Hdac9
O
IP
Input
IgG
Foxp3
Mef2d
Mef2d
Foxp3

Figure 1. Foxp3 controls *Mef2d* transcription and influences MEF2D protein-protein interactions. (**A**) qPCR results in Treg and Teff cells from WT mice ($n = 4$, *t* test). (**B**) Immunoblots of the indicated proteins in Treg and Teff (Te) cells from WT mice. (**C**) Diagram of phosphorylation sites retained or lost in MEF2Dα1 and -α2 isoforms. (**D**) qPCR in freshly isolated WT Teffs and Tregs or cells cultured under activating conditions for 24 hours (1:1 ratio anti-CD3/anti-CD28 mAb–coated beads); $n = 6$, Tukey's multiple-comparison test. (**E**) Immunoblots of the indicated proteins in the same cells as described in **D**. (**F**) Densitometric analysis relative to **E**; $n = 2$, *t* test relative to Teffs. (**G**) qPCR results of *Mef2d* (pan, α1, α2) expression in freshly isolated WT Teffs and Tregs or cultured under activating conditions for 60 hours in the presence of 5 μM scrambled or Foxp3 antisense (as) oligonucleotide; $n = 3$, Tukey's multiple-comparison test. (**H**) Immunoblots of the indicated proteins in the same cells as described in **G**. (**I**) Densitometric analysis relative to **H**. $n = 2$, *t* test relative to scrambled. (**J**) HEK293T cells were transfected with 1 μg each of tagged constructs encoding Foxp3, MEF2D, and p300; lysates were pulled down with anti-Myc or IgG Ab (1 μg). The membrane was probed with biotinylated anti-Foxp3 mAb, anti-HA for p300, and anti-Myc for MEF2D. (**K**) HEK293T cells were transfected with 1 μg each of FLAG-Foxp3 and the depicted deletion mutants of MEF2D-GFP. Lysates were pulled down with anti-GFP Ab (1 μg). (**L**) Lysates from freshly isolated or 24-hour anti-CD3/anti-CD28–stimulated Teffs and Tregs were pulled down with anti-MEF2D or IgG Ab (1 μg). (**M**) Lysates from freshly isolated Tregs were pulled down with anti-MEF2Dα1 or anti-MEF2Dα2 or IgG Ab (1 μg). (**N**) HEK293T cells were transfected with 1 μg each of tagged constructs encoding Foxp3, MEF2Dα1, MEF2Dα2, and Hdac9. Lysates were pulled down with anti-MEF2Dα1, -Mα2, or IgG Ab (1 μg). (**O**) Lysates from freshly isolated Tregs were pulled down with anti-Foxp3 or IgG Abs (1 μg); 1/50 input included in all the IPs. Asterisks in panels **K**, **L**, and **O** indicate heavy chains of IgG Abs used in pull-down experiments. $^*P < 0.05$; $^{**}P < 0.01$; $^{***}P < 0.005$.

cells (Figure 2, D and E). Although no significant alterations were observed in $CD8^+$ subpopulations (data not shown), increased proportions of $CD4^+Foxp3^-$ effector memory cells ($CD44^{hi}CD62L^{lo}$) were observed within lymph nodes, spleen, and thymus (Figure 2, F and G). Nevertheless, the in vitro suppressive functions of Tregs from *Mef2d*$^{-/-}$ mice were not significantly impaired compared with WT Tregs in standard Treg assays (Figure 2, H and I), though they did display modestly impaired suppression of $CD4^+$ and $CD8^+$ cells when using bulk WT splenocytes as responder cells (Figure 2J). Altogether, these features are indicative of a modest inflammatory state in *Mef2d*$^{-/-}$ mice but one that is insufficient to provoke significant autoimmunity under basal conditions.

MEF2D-specific and Foxp3-specific signatures are altered in Mef2d$^{-/-}$ *Tregs*. The transcriptomes of WT and *Mef2d*$^{-/-}$ Tregs were analyzed by RNA sequencing (RNA-seq). Mef2d deletion caused the upregulation of 795 transcripts and the repression of 700 genes (>1.3-fold, $P < 0.05$) (Figure 3A). Gene set enrichment analysis (GSEA) showed that 4 main signaling pathways were altered in *Mef2d*$^{-/-}$ Tregs: (i) DNA repair (Figure 3B and Supplemental Figure 3A), (ii) E2F targets/proliferation (Figure 3C and Supplemental Figure 3B), (iii) PPAR/RA signaling (Figure 3D and Supplemental Figure 3C), and (iv) Treg signature (Figure 3, E and F, and Supplemental Figure 3, D and E). The first 3 were severely impaired in *Mef2d*$^{-/-}$ Tregs and belong to the general core responses regulated by MEF2 transcription factors (22). Analysis of the Treg signature (42) showed that key genes induced in Treg versus Teff cells were indeed repressed in *Mef2d*$^{-/-}$ Tregs (Figure 3E), and conversely, transcripts normally repressed in Tregs were upregulated in *Mef2d*$^{-/-}$ Tregs (Figure 3F). We validated by qPCR (Figure 3H) and immunoblot (Figure 4A) changes in expression the main hubs involved in the identified altered pathways. We confirmed by different methods an impairment in the proliferation of *Mef2d*$^{-/-}$ Tregs (Figure 4, B–D and Supplemental Figure 4, A–C) that appears at least partially due to a prolonged quiescence rather than senescence (Figure 4C), even if a moderate impairment in cellular fitness cannot be excluded.

Mef2d$^{-/-}$ *Tregs lose the hallmarks of eTregs*. Foxp3 was expressed in *Mef2d*$^{-/-}$ Tregs at levels comparable to those of control mice (Figure 4A). However, *Mef2d*$^{-/-}$ Tregs showed reduced levels of 3 genes (*Ctla4*, *Icos*, and *Il10*) that encode proteins centrally involved in the immunosuppressive functions of Tregs (Figure 3G and Figure 4A). High levels of these proteins are a feature of so-called highly suppressive eTregs (43) that are dependent on Blimp1 (21) and Irf4 (44). GSEA performed on the transcriptome of *Mef2d*$^{-/-}$ Tregs confirmed their inverse correlation with $Blimp1^+$ Tregs (Figure 5, A and B); in particular, key genes induced in $Blimp1^+$ cells were significantly repressed in *Mef2d*$^{-/-}$ Tregs (Figure 5C). We validated by qPCR (Figure 3G) and flow cytometry (Figure 5, D–F and Supplemental Figure 4F) the downregulation in *Mef2d*$^{-/-}$ Tregs of CTLA4, Icos, and IL-10; the latter is especially impressive in stimulated cells (Figure 5G). As a consequence, Teff cells were more active in *Mef2d*$^{-/-}$ mice (Figure 2, F and G).

Blimp1 expression was not altered in *Mef2d*$^{-/-}$ cells (Figure 5H), and *Mef2d* expression was not altered in *Blimp1*$^{-/-}$ Tregs (GSE84827, Supplemental Figure 5A) (45). Moreover, Blimp1 does not interact with MEF2D, but does pull down its well-known interactor, Hdac2 (46) (Supplemental Figure 5B). However, Hdac9 is repressed in $Blimp1^+$ Tregs (GSE103456, Supplemental Figure 5C) (47) and is induced in *Blimp1*$^{-/-}$ Tregs (GSE84827, Supplemental Figure 5A) (45). This suggests that in $Blimp1^+$ Tregs, MEF2D is released from its inhibitors. Indeed, many Blimp1 target genes are bound by MEF2 at their proximal promoters (Table 1). We hypothesized that MEF2D acts downstream of Blimp1 and is required to sustain the high repressive properties of eTregs. As expected, the suppressive properties of $Foxp3^+$ *Mef2d*$^{-/-}$ Tregs were only partially enhanced after their preactivation with anti-CD3/anti-CD28, differently from WT (Figure 5, I and J). This defect may be partially due to a moderately increased susceptibility of *Blimp1*$^{-/-}$ Tregs to apoptosis, as seen in vitro (Supplemental Figure 5, D and E). These features, collectively, are typically associated with an impairment of eTreg functions (48). A similar trend was also seen in Tregs, expanded in vivo by IL-2, in Treg assays (Supplemental Figure 5, F–I).

Conditional Treg deletion of Mef2d affects Tfr and Tfh cells and B cell maturation in germinal centers. MEF2D acts upstream of CTLA4 and downstream of Blimp1 in regulating Treg suppressive properties. As CTLA4 (18) and Blimp1 (19) are key regulators of Tfr functions and B cell responses, we investigated whether *Mef2d* deletion in $Foxp3^+$ cells would affect Tfr and Tfh responses. Similarly to CTLA4 and Blimp1, *Mef2d* KO showed increased Tfr and Tfh cells (Figure 6, A and B). While the total numbers of B cells, memory B cells, and plasma cells were not altered (Figure 6C), increased numbers of B1 (Figure 6D), follicular type I B (Figure 6E), transitional T3 B (Figure 6H), and germinal center (GC) (Figure 6I) B cells were observed in *Mef2d*$^{-/-}$ mice. The rise in follicular type I B cells and the corresponding drop in marginal

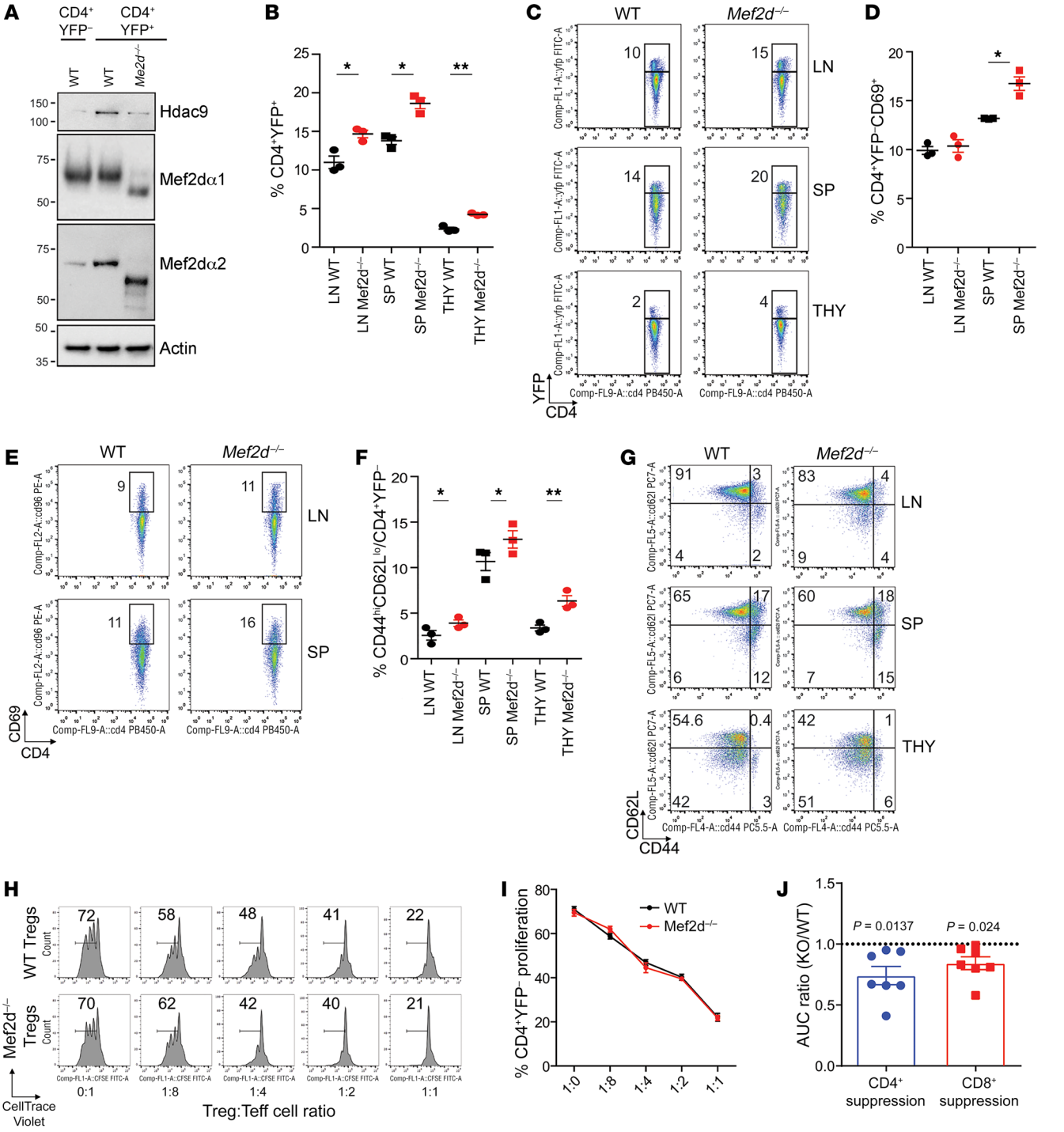

Figure 2. Generation and characterization of mice with conditionally deleted *Mef2d* in Foxp3⁺ Treg cells. (**A**) Immunoblots of MEF2Dα1 and -α2 and Hdac9 in freshly isolated Teffs and Tregs obtained from WT and *Mef2d*$^{-/-}$ mice, as indicated; β-actin served as loading control. (**B** and **C**) Analysis of CD4⁺Foxp3⁺ cells in lymphoid tissues from *Mef2d*$^{-/-}$ or WT mice (n = 3); the experiment was repeated 2 times with 3 mice/group with similar results. *P < 0.05, **P < 0.01 by t test. LN, lymph nodes; SP, spleen, THY, thymus. (**D**–**G**) Analysis of CD4⁺CD69⁺ and CD4⁺CD44^{hi}CD62L^{lo} cells in CD4⁺YFP⁻ populations in lymphoid tissues from *Mef2d*$^{-/-}$ or WT mice (n = 3); the experiment was repeated 2 times with 3 mice/group with similar results. *P < 0.05, **P < 0.01 by t test. (**H** and **I**) In vitro Treg suppression assay using pooled (4 mice/group) Tregs from lymph nodes and spleens of *Mef2d*$^{-/-}$ or WT mice and WT T cells; the percentage of WT proliferating cells is shown in each panel. The experiment was run in triplicate and repeated at least 3 times, and the results of one representative experiment are shown. (**J**) AUC ratios (KO/WT, 1-sample t test with theoretical mean = 1) of 3 Treg suppression assays performed on CFSE-labeled WT splenocytes as responder cells. The suppressive effects on CD4⁺ and CD8⁺ responder cells were evaluated after CD4 and CD8 immunostaining.

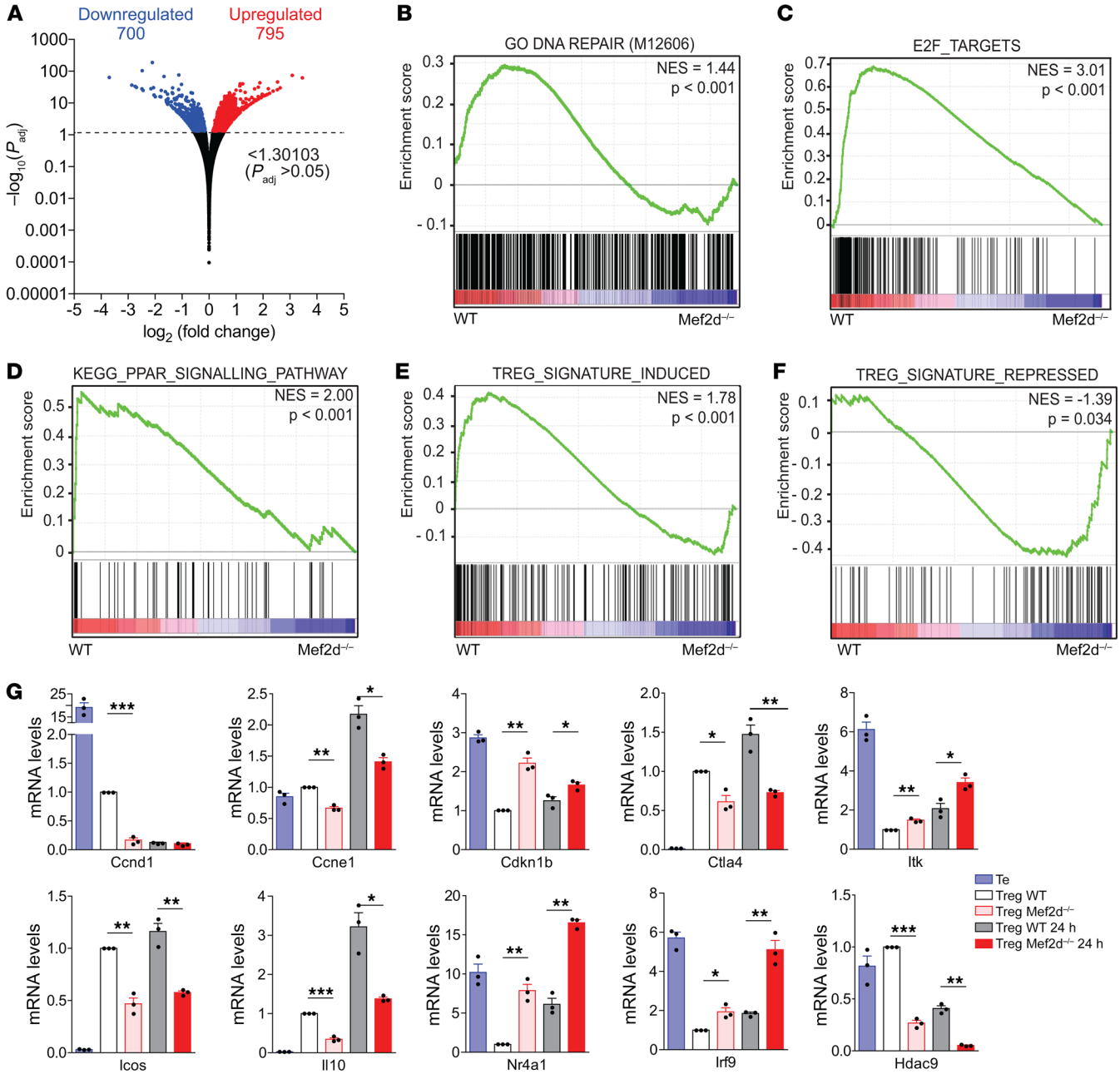

Figure 3. *Mef2d* deletion affects general and Foxp3-specific responses. (**A**) A volcano plot showing statistical significance (*P* value) versus fold change for genes differentially expressed as a result of *Mef2d* deletion in Foxp3$^+$ Treg cells. (**B**–**F**) GSEA plots obtained by using the indicated gene sets and the RNA-seq data obtained from the comparison between *Mef2d*$^{-/-}$ or WT mice Tregs as data set. (**G**) qPCR results of the expression of the indicated genes in freshly isolated *Mef2d*$^{-/-}$ or WT Teffs (TE) and Tregs or cultured under activating conditions for 24 hours (1:1 ratio of anti-CD3/anti-CD28 mAb–coated beads); $n = 5$. $^*P < 0.05$, $^{**}P < 0.01$, $^{***}P < 0.005$ by *t* test between Teffs and Tregs in unstimulated and stimulated groups.

zone precursors (Figure 6, F and G) observed after MEF2D depletion suggest an enhancement of B cell receptor (BCR) signals (49). The expansion of the GC and the alteration of BCR signaling indicate increased GC reactions. Consistent with that, moderate levels of autoantibodies were found in *Mef2d*$^{-/-}$ mice (Figure 6J and Supplemental Figure 5J).

Mef2d deletion dampens Treg function in vivo. As we predicted that Tregs require MEF2D to acquire the features of highly suppressive eTregs, we established 3 animal models to assess the effects of *Mef2d* deletion on Tregs in vivo.

First, we tested the strength of *Mef2d*$^{-/-}$ Tregs to inhibit homeostatic proliferation of CD4$^+$ and CD8$^+$ T cells over 28 days following their adoptive transfer into *Rag1*$^{-/-}$ mice (30). In comparison with WT Tregs, *Mef2d*$^{-/-}$ Tregs were severely impaired in their capability to suppress the proliferation of CD4$^+$ Teffs in the lymph nodes (Figure 7A). In addition, upon activation they produced more IFN-γ (Figure 7B and Supplemental Figure 6A) and IL-2 (Figure 7C and Supplemental Figure 6B). No differences were observed in the spleen (Figure 7, A and F and Supplemental Figure 6E), even though *Mef2d*$^{-/-}$ Tregs were less activated in both

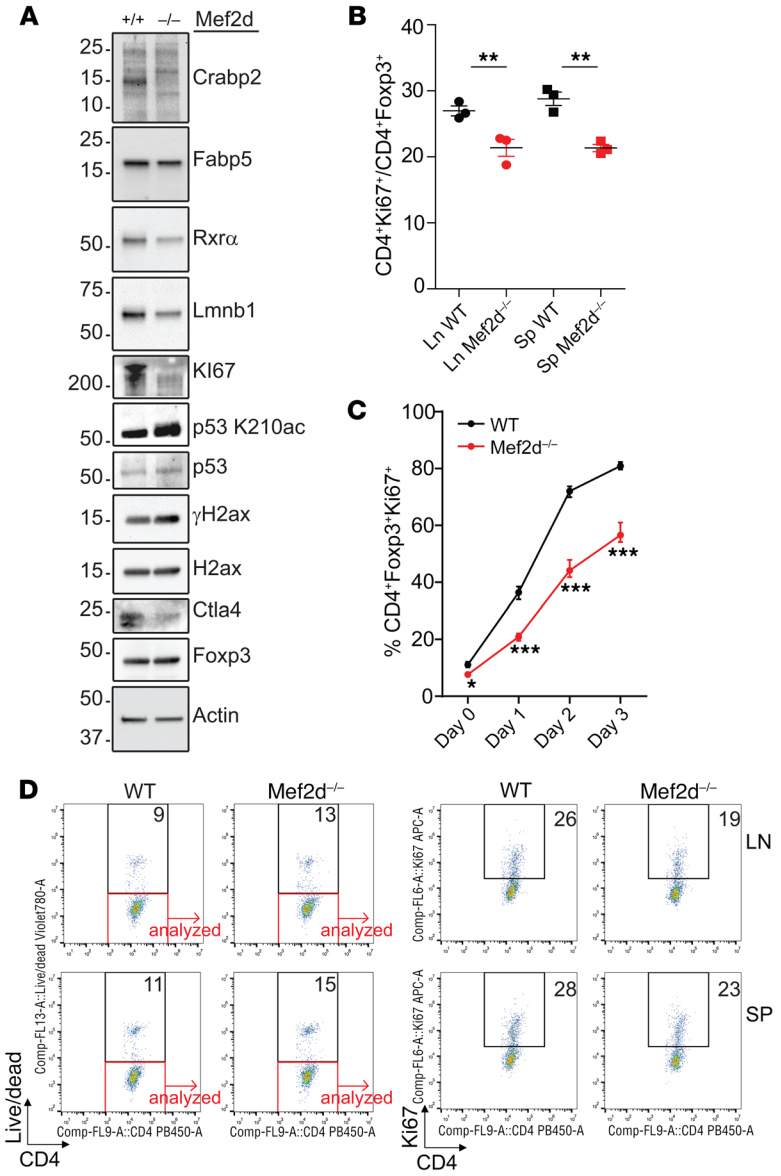

Figure 4. *Mef2d* deletion perturbs the fitness of Tregs. (**A**) Immunoblots of the expression of the indicated proteins representing key nodes in the identified perturbed pathways in freshly isolated Teffs and Tregs obtained from *Mef2d*$^{-/-}$ or WT mice, as indicated. β-Actin was used as loading control. (**B** and **D**) Analysis of CD4$^+$Ki67$^+$ in CD4$^+$Foxp3$^+$ populations in lymphoid tissues from *Mef2d*$^{-/-}$ or WT mice. $n = 3$. $^{**}P < 0.01$ by t test. (**C**) Time course analysis of Ki67 positivity in CD4$^+$Foxp3$^+$ populations purified from *Mef2d*$^{-/-}$ or WT mice and kept in culture for 3 days with anti-CD3/anti-CD28 mAb–coated beads; $n = 4$. $^{*}P < 0.05$, $^{***}P < 0.005$ by t test between the 2 groups for each time point.

spleen and lymph nodes (Figure 7D and Supplemental Figure 6C). Increased proportions of *Mef2d*$^{-/-}$ Tregs were found among the splenocytes but not in lymph nodes (Figure 7E and Supplemental Figure 6D) and this was not due to altered expression of chemokine receptors (Supplemental Figure 6F) or changes in proliferation (Supplemental Figure 4, D and E). Finally, *Mef2d*$^{-/-}$ Tregs were found to be even more strongly impaired in their ability to repress CD8$^+$ T cell proliferation and/or survival (Figure 7, G and H).

Second, we performed cardiac allografting using BALB/c donors and WT or *Mef2d*$^{-/-}$ C57BL/6 recipients in conjunction with costimulation blockade with anti-CD40L (CD154) mAb plus donor splenocyte transfusion (49). Costimulation blockade induced long-term allograft survival (>100 days) in WT recipients but not in mice with conditional deletion of *Mef2d* within their Treg cells ($P < 0.01$) (Figure 7I). The acute rejection observed in *Mef2d*$^{-/-}$ mice correlated with CD8$^+$ T cell activation and intragraft expression of IFN-γ and granzyme B (GZMB) (Figure 7J) and an impairment of Tregs (Figure 7K). Histologic examination of allografts in *Mef2d*$^{-/-}$ recipients collected just before end-stage rejection at 16 days after transplant (post-Tx) showed marked differences from allografts harvested from WT recipients at the same post-Tx interval (Supplemental Figure 7). The latter showed well-preserved myocardium and vessels and small numbers of mononuclear cells palisading within capillaries and occasional interstitial areas. In contrast, allografts in *Mef2d*$^{-/-}$ mice showed widespread myocyte necrosis and vascular injury with fibrointimal proliferation, mixed mononuclear and polymorphonuclear infiltrates, and interstitial hemorrhages. Rejecting allografts also showed vascular deposition of C4d (Supplemental Figure 8). Collectively, these findings in *Mef2d*$^{-/-}$ recipients are consistent with increased host cellular and humoral alloresponses.

Third, as shown next, we studied the effects of deletion of *Mef2d* in Tregs on host antitumor immunity.

Mef2d deletion promotes antitumor immunity. We used 3 models involving tumor growth in syngeneic mice; 2 lung cancer cell lines (TC1 and AE.17) were injected subcutaneously, and a hepatocellular carcinoma (HCC) cell line was delivered by injection of the mesenteric vein.

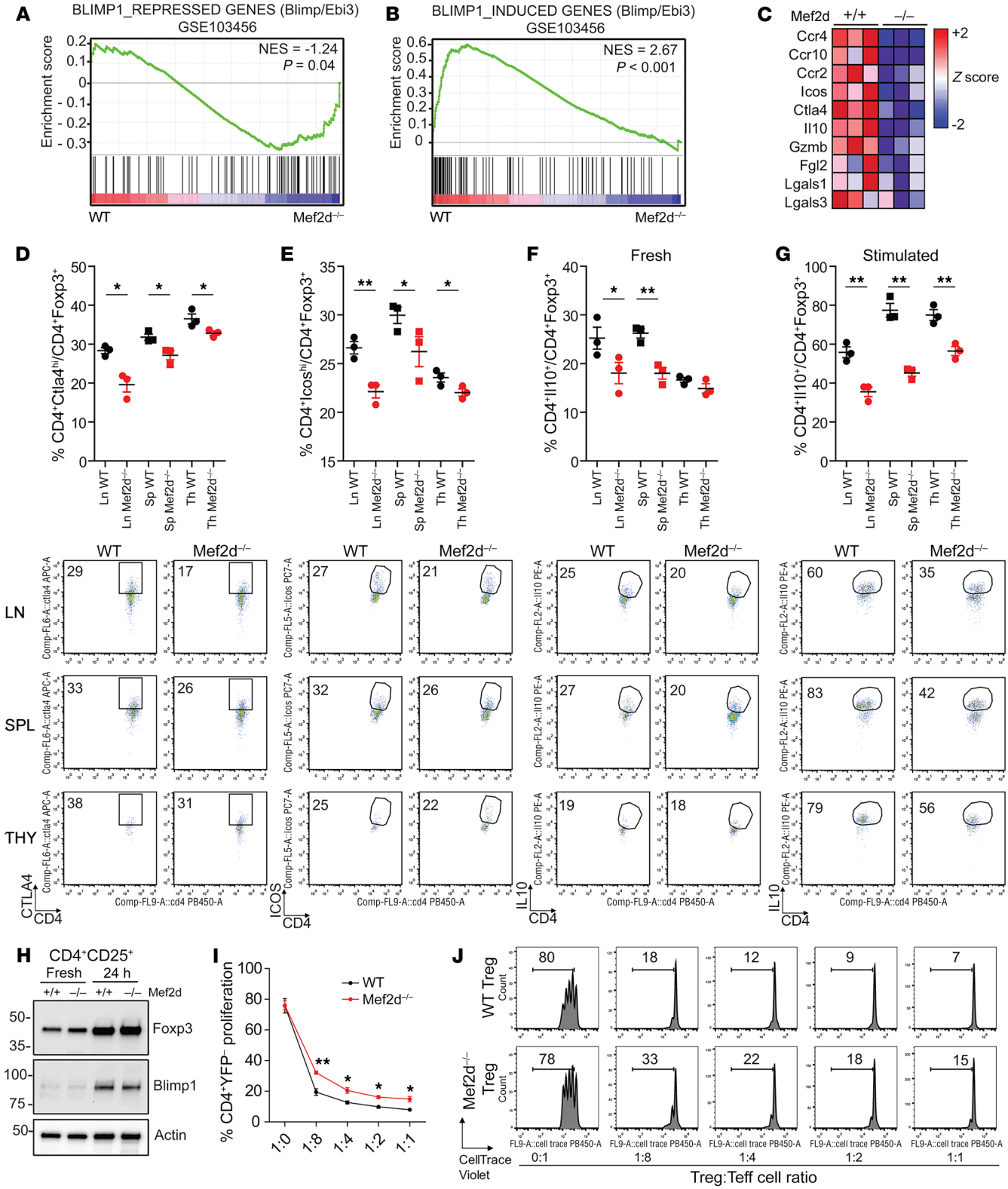

Figure 5. MEF2D is required for the acquisition by Tregs with highly suppressive properties. (**A** and **B**) GSEA plots obtained by using the indicated gene sets and the RNA-seq data obtained from the comparison between *Mef2d*$^{-/-}$ or WT Tregs as data set. (**C**) Heatmap of the expression levels (*Z* scores) of 10 core genes upregulated in Blimp1^{+} *Mef2d*$^{-/-}$ or WT Tregs. (**D**–**G**) Analysis of CD4^{+}Foxp3^{+}CTLA4^{hi} (**D**), CD4^{+}Foxp3^{+}Icos^{hi} (**E**), and CD4^{+}Foxp3^{+}IL-10^{+} (**F** and **G**) populations in lymphoid tissues from *Mef2d*$^{-/-}$ or WT mice, freshly isolated (**D** and **F**) or stimulated with PMA/ionomycin for 4 hours (**G**); the experiment was repeated 2 times, with 3 mice/group, with similar results. **P* < 0.05, ***P* < 0.01 by *t* test between WT and KO samples. (**H**) Immunoblots of Blimp1 and Foxp3 in freshly isolated or 24-hour anti-CD3/anti-CD28–stimulated Tregs obtained from *Mef2d*$^{-/-}$ or WT mice, as indicated; β-actin was used as loading control. (**I** and **J**) Representative Treg suppression assay and pooled data (3 mice/group) using Tregs from lymph nodes and spleens of *Mef2d*$^{-/-}$ or WT mice along with the percentage of proliferating cells in each panel; 48 hours before assay, *Mef2d*$^{-/-}$ or WT Tregs were isolated and stimulated with 1:1 anti-CD3/anti-CD28–coated beads and 10 U/mL IL-2. **P* < 0.05, ***P* < 0.01 by *t* test between the 2 groups for each condition.

Table 1. Top 10 transcription factors (TFs) binding Blimp1-regulated genes

TF	*Z* score	*P* value
NF-κB	1.76	0.003
STAT5	1.67	0.001
POU2F2	1.67	0.009
BATF3	1.66	0.005
RUNX3	1.66	0.028
PAX5	1.61	0.001
MEF2	1.61	0.003
FOXP1	1.59	0.004
TBX21	1.59	0.005
BCLAF1	1.56	0.008

Z scores and *P* values were retrieved from BART (http://faculty.virginia.edu/zanglab/bart/) and refer to the ChIP-seq data deposited in ENCODE.

The growth of TC1 cells was profoundly impaired in *Mef2d*$^{-/-}$ mice; in 9 of 10 mice the tumors were almost completely cleared (Figure 8A), in conjunction with activation (Figure 8, B and C) and IFN-γ production by CD4$^+$ (Figure 8, D and E) and CD8$^+$ (Figure 8, F–I) T cells in the tumor-draining lymph nodes. Compared with WT tumor-bearing mice, *Mef2d*$^{-/-}$ mice had increased activation of CD4$^+$ Teffs (CD44^{hi}CD62L^{lo}; Figure 8, B and C) that was inversely correlated with the impairment in Treg functions (IL-10 production, CTLA4 and Ki67 expression; Supplemental Figure 9, A–F). Moreover, Tregs harvested from the tumor-draining lymph nodes showed evidence of transcriptome alterations (Supplemental Figure 9G) consistent with that of Tregs in non–tumor-bearing *Mef2d*$^{-/-}$ mice (Figure 3G). The infiltration of Tregs in TC1 tumors was assessed after 8 days, so as to precede shrinking of the tumors. *Mef2d*$^{-/-}$ Tregs infiltrated the tumor as well as WT Tregs (Figure 8K). However, tumor-infiltrating CD4$^+$ and CD8$^+$ T cells were more numerous and more activated in *Mef2d*$^{-/-}$ mice (Figure 8, K and L, and Supplemental Figure 9H), likely as a consequence of impaired Treg functions (Supplemental Figure 9, A–F). The increased numbers of HPV/TC1-specific tetramer-positive CD8$^+$ T cells in *Mef2d*$^{-/-}$ mice suggests that the activation of CD8$^+$ T cells was tumor specific (Figure 8J). Similarly to TC1, the growth of AE.17 tumors was impaired in *Mef2d*$^{-/-}$ mice (Figure 8M), and again the proportions of activated and IFN-γ–producing CD8$^+$ (Figure 8N and Supplemental Figure 9I) and CD4$^+$ (Supplemental Figure 9, J and K) T cells were increased within the tumor-draining lymph nodes.

Finally, the injection of HCC cells via the mesenteric vein, after 9 days gave rise to histologically confirmed liver tumors in 7 of 10 WT mice but in only 2 of 10 *Mef2d*$^{-/-}$ littermates (Figure 9A). As the tumors differed markedly in the number and dimensions of the lesions, we used α-fetoprotein (AFP) levels in the serum as a read-out of tumor growth (50). In C57BL/6 mice, levels of serum AFP greater than 200 ng/mL correlated with HCC growth (50). Serum AFP levels in WT mice were significantly higher than in *Mef2d*$^{-/-}$ mice or in C57BL/6 mice not injected with HCC cells (median values ± SE: C57BL/6 healthy, 60.6 ± 8.1; WT HCC, 204.5 ± 21.5; *Mef2d*$^{-/-}$ HCC, 122.3 ± 17.9) (Figure 9B). In *Mef2d*$^{-/-}$ mice, conventional CD4$^+$ cells were more active (CD44^{hi}CD62L^{lo} and CD69$^+$, Figure 9, C and D; and Supplemental Figure 10, A and B), produced more IFN-γ (Figure 9E and Supplemental Figure 10C), and were more proliferative (Figure 9F and Supplemental Figure 10D). Conversely, the Treg population was less proliferative (Figure 9G and Supplemental Figure 10E) and was characterized by lower levels of CTLA4 (Figure 9H and Supplemental Figure 10F) and IL-10 (Figure 9I and Supplemental Figure 10G). The alterations in the transcriptome (Figure 9J) and in the proteome (Figure 9K) typical of *Mef2d*$^{-/-}$ Tregs were maintained or became even greater in HCC-bearing mice. No significant differences were observed in the CD8$^+$ population (Supplemental Figure 10, H and I) or in the production of IL-2 by CD4$^+$ cells (Supplemental Figure 10J). Comparable data illustrating the marked inhibitory effects of *Mef2d* deletion in Tregs on HCC tumor growth were seen on day 21 after injection (Supplemental Figure 11).

MEF2D assembles repressive and activating complexes to maintain Treg immunosuppressive properties. To gain more insight into the mechanisms elicited by MEF2D in sustaining Treg suppressive properties, we performed ChIP using freshly isolated WT and *Mef2d*$^{-/-}$ Tregs. We mapped the binding of MEF2D with 3 different Abs (specific for α1, α2, and a pan-Ab to IP both isoforms) on the more relevant genomic loci identified as being under the control of MEF2D. We mapped in the same loci Foxp3 and p300, while the comparison of H3K27ac levels between WT and *Mef2d*$^{-/-}$ Tregs provided a read-out of the positive or negative transcriptional activities of the investigated complexes. In the case of *Ctla4/Icos* we investigated 7 regions that bear MEF2 binding sites and/or were previously pulled down by Foxp3 in ChIP experiments (Supplemental Figure 12A, Figure 10, A–G). Foxp3 significantly bound the proximal promoter (region A) and an intronic region (region D) of *Ctla4* (Figure 10, A and D). We did not find significant coassociation of MEF2D in these chromatin positions, while both MEF2Dα1 and MEF2Dα2 precipitated the intronic region C (Figure 10C). A decrease in H3K27ac levels in *Mef2d*$^{-/-}$ Tregs was observed in the proximal promoter (region A) and in the intronic region C (Figure 10, A and C); in these positions a significant drop in p300 binding was observed (Figure 10, A and C). MEF2D (pan and MEF2D α2 isoform) and Foxp3 were coassociated at the *Icos* promoter (region G); this region was characterized by decreased H3K27ac in *Mef2d*$^{-/-}$ cells (Figure 10G), while a drop in p300 binding was also observed at the distal promoter (region F; Figure 10F). MEF2D was previously described as a positive regulator of *Il10* transcription in T cells (51, 52) and in glial cells (53), through direct binding to the proximal promoter (53). We confirmed binding of MEF2D (α1, α2, and pan) to the proximal promoter of *Il10*, in association with p300 but in the absence of Foxp3 (Figure 10H). In *Mef2d*$^{-/-}$ Tregs, decreased levels of p300 binding and H3K27ac were observed (Figure 10H). MEF2D was associated with the *Nr4a1* promoter (Figure 10I), as observed in other contexts (29, 54–57); the same region is bound by Foxp3 (Figure 10I) and p300. In this locus, MEF2D appeared to form a repressive complex, as the KO had increased p300 binding and H3K27ac (Figure 10I). MEF2D was found to be significantly associated with the *Hdac9* promoter (Figure 10J), used as a positive control. Finally, MEF2D also repressed the transcription of *Itk*, without perturbing p300 binding but reducing levels of H3K27ac at the promoter level, probably by promoting the engagement of

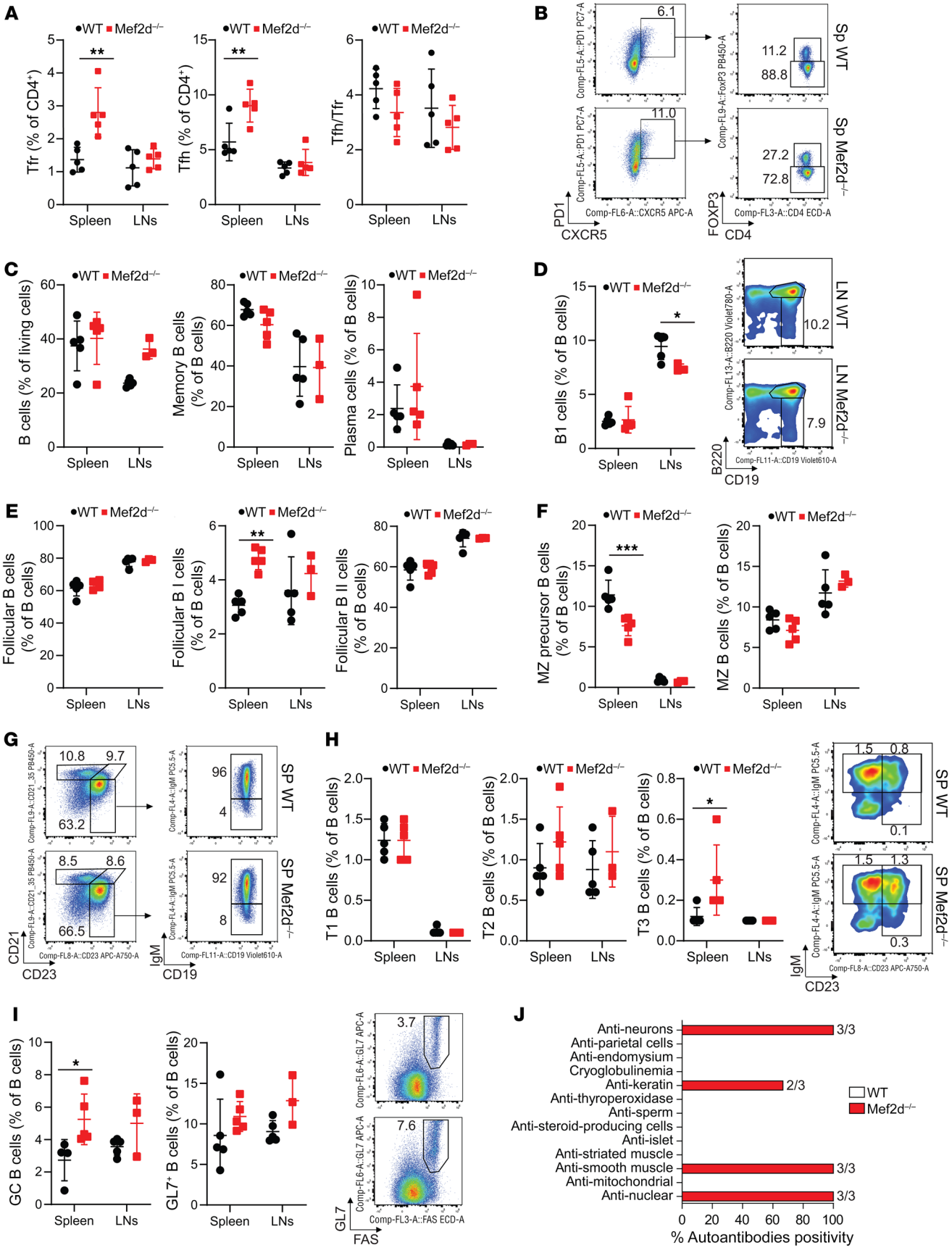
A
WT Mef2d−/−
Tfr (% of CD4+)
Tfh (% of CD4+)
Tfh/Tfr
Spleen
LNs
B
Sp WT
Sp Mef2d−/−
6.1
11.2
88.8
11.0
27.2
72.8
PD1
CXCR5
FOXP3
CD4
C
B cells (% of living cells)
Memory B cells (% of B cells)
Plasma cells (% of B cells)
D
B1 cells (% of B cells)
LN WT
LN Mef2d−/−
10.2
7.9
B220
CD19
E
Follicular B cells (% of B cells)
Follicular B I cells (% of B cells)
Follicular B II cells (% of B cells)
F
MZ precursor B cells (% of B cells)
MZ B cells (% of B cells)
G
10.8
9.7
63.2
8.5
8.6
66.5
96
4
92
8
CD21
CD23
IgM
CD19
H
T1 B cells (% of B cells)
T2 B cells (% of B cells)
T3 B cells (% of B cells)
1.5
0.8
0.1
1.3
0.3
I
GC B cells (% of B cells)
GL7+ B cells (% of B cells)
3.7
7.6
GL7
FAS
J
Anti-neurons
Anti-parietal cells
Anti-endomysium
Cryoglobulinemia
Anti-keratin
Anti-thyroperoxidase
Anti-sperm
Anti-steroid-producing cells
Anti-islet
Anti-striated muscle
Anti-smooth muscle
Anti-mitochondrial
Anti-nuclear
3/3
2/3
3/3
3/3
WT
Mef2d−/−
% Autoantibodies positivity

Figure 6. *Mef2d* deletion dampens Tfr functions partially affecting the Tfh-mediated regulation of B cell maturation. (**A** and **B**) Analysis of Tfr ($CD4^+CXCR5^+PD\text{-}1^+Foxp3^+$) and Tfh ($CD4^+CXCR5^+PD\text{-}1^+Foxp3^-$) populations in lymphoid tissues from *Mef2d*$^{-/-}$ or WT mice. $n = 5$. $^{**}P < 0.01$ by *t* test between WT and KO samples. (**C**) Analysis of B cell ($CD19^+$), memory B cell ($CD19^+B220^+CD62^{lo/-}FAS^-GL7^-CD138^-$), and plasma cell ($CD138^+IgM^-$) populations in lymphoid tissues from *Mef2d*$^{-/-}$ or WT mice. $n = 5$; *t* test between WT and KO samples. (**D**–**I**) Analysis of B cell subpopulations in lymphoid tissues from *Mef2d*$^{-/-}$ or WT mice. (**D**) B1 cells ($B220^-CD19^+$); (**E**) follicular B cells ($CD19^+B220^+CD93^-CD21^{lo}CD23^{hi}$), follicular B type I cells ($CD19^+B220^+CD93^-CD21^{lo}CD23^{hi}IgM^{lo}$), follicular B type II cells $CD19^+B220^+CD93^-CD21^{lo}CD23^{hi}IgM^{hi}$); (**F**) marginal zone (MZ) precursor B cells ($CD19^+B220^+CD93^-CD21^{hi}CD23^{lo}$) and MZ B cells ($CD19^+B220^+CD93^-CD21^{hi}CD23^{hi}$); (**H**) transitional type 1 (T1) B cells ($CD19^+B220^+CD93^+IgM^{++}CD23^-$), T2 B cells ($CD19^+B220^+CD93^+IgM^{++}CD23^+$), and T3 B cells ($CD19^+B220^+CD93^+IgM^-CD23^+$); (**I**) GC B cells ($CD19^+B220^+GL7^+FAS^+$) and $GL7^+$ activated B cells ($CD19^+B220^+GL7^+$). $n = 5$. $^*P < 0.05$, $^{**}P < 0.01$, $^{***}P < 0.001$ by *t* test between WT and KO samples. (**J**) Autoantibodies detected in the sera of 3 WT and 3 *Mef2d*$^{-/-}$ mice, using indirect immunofluorescence.

Foxp3 (Figure 10K). Among the genes bound and regulated by MEF2D in Tregs, some (*Hdac9* and *Il10*) were also under MEF2D control in Teffs (Figure 10L and Supplemental Figure 12, B and C), as well as in non-lymphoid organs and cell types (24, 34, 38, 52, 54, 56). Others, like *Icos* and *Ctla4,* were Treg restricted, probably because MEF2D binding requires the establishment of a permissive open chromatin status (Figure 10L and Supplemental Figure 12, B and C), primed by Foxp3.

In summary, MEF2D established both repressive and activating complexes on relevant loci for Treg homeostasis and immune-suppressive functions. In some cases, its binding was directly assisted by Foxp3 (*Icos* promoter region G and *Nr4a1*); in a second group of loci (*Ctla4* region C) MEF2D assisted the transcription proficiency stimulated by Foxp3, while in others the MEF2D transcriptional effect was Foxp3 independent (*Il10* and *Hdac9*). The activating or repressive functions of MEF2D depend on the corepressors or coactivators recruited to chromatin. We observed perfect correlation between H3K27ac, p300, and the transcriptional activity in all the examined loci, except for *Itk*, which appeared to be regulated through an indirect mechanism.

Discussion

MEF2 transcription factors regulate differentiative and adaptive/stress-related responses (22). In mammals, MEF2D is the most ubiquitously expressed of the 4 paralogs, being abundant in almost all tissues and cell types (22). This wide expression pattern reflects the key roles of MEF2D in regulating general responses involved in maintaining cellular fitness, including the control of cell-cycle progression, mitochondrial activity, and the balance of prosurvival and apoptotic responses (22, 41). However, MEF2D also has tissue- and cell-type specific functions, like the promotion of muscle differentiation, remodeling, regeneration, and the control of neuronal development and synaptogenesis (22, 41). Moreover, MEF2D controls the development of particular cell types, like retina photoreceptors (58). Three mechanisms allow MEF2D to exert context-dependent biological functions: (i) the plasticity of MEF2D-containing complexes and the coexistence in the same cell of MEF2 transcriptional activator and repressor complexes (38), (ii) the ability to bind chromatin away from its traditional consensus sites thanks to MEF2 binding to lineage-specific transcription factors (58), and (iii) the expression of cell-specific MEF2 isoforms that display differential affinity for cofactors (33, 36).

We found that all 3 of these mechanisms are operative in Tregs. The expression of Foxp3 triggers the alternative splicing mechanism that gives rise to the α2 isoform of MEF2D. This isoform is refractory to the binding to class IIa Hdacs and Hdac9, in particular, and has higher affinity for Foxp3. The α1 isoform retains a reduced capability to interact with Foxp3 and a stronger affinity for Hdacs. The copresence of the 2 isoforms sustains the expression of Treg-specific genes, maintaining the balance between the establishment of activating and repressive transcriptional complexes. We observed that in Tregs, MEF2D and Foxp3 can act synergistically (on *Icos* and *Nr4a1* loci), additively (on *Ctla4* and *Il10*), or independently (on *Itk* and *Hdac9*). A fine regulation of this balance ensures the maintenance of the highly suppressive properties of Tregs. In particular, *Mef2d*$^{-/-}$ Tregs fail to generate eTreg cells. MEF2D appears to be downstream of Blimp1, the main regulator of IL-10$^+$ eTregs (21), as the core of Blimp1-regulated genes (47) show evidence of MEF2 binding at their promoters. Moreover, as Blimp1 directly controls only 8% of the eTreg signature (59), we can now identify MEF2D among the transcription factors involved in sustaining the eTreg phenotype.

In fact, while *Mef2d*$^{-/-}$ Tregs were only slightly impaired in their suppressive functions in vitro, they were severely impaired in repressing the proliferation of $CD4^+$ and $CD8^+$ T cells in vivo. Moreover, the activation of $CD4^+$ and $CD8^+$ T cells after the depletion of *Mef2d* in Tregs induced allograft rejection and promoted antitumor immunity, as seen in 3 different cancer models (HCC and lung) known for being Treg dependent in vivo (60–62). Interestingly, in HCC and in non–small cell lung carcinoma, as in various tumors, MEF2D expression is increased and reported to be required to sustain tumor growth (63–65). The upregulation of PD-L1 frequently observed in HCC has been correlated to the impairment of CD8-mediated cytotoxicity (66) and could explain the inefficient activation of $CD8^+$ lymphocytes observed in this model in *Mef2d*$^{-/-}$ mice. As MEF2D was found to control the expression of PD-L1 (67), in these cancers a targeted therapy to inhibit MEF2D functions could have a double benefit of decreasing the malignancy of tumor cells and increasing the immunoreactivity of T cells. Regarding this, small molecules that target the interaction of MEF2 with class IIa Hdacs have been reported (65, 66).

The lack of signs of severe inflammation or autoimmunity in mice depleted of *Mef2d* in Foxp3$^+$ Tregs is in line with the effects of deletion of *Blimp1* (45), *Icos* (67), and *Il10* (68). In the latter, no autoimmunity but mild colitis was reported (68), while *Prdm1*$^{-/-}$ mice display marks of autoimmunity only in aging mice (59). Moreover, similarly to *Mef2d*, the ablation of *Blimp1*, *Icos*, *Il10*, or *Ctla4* in Tregs does not impact their suppressive properties in vitro, but impairs their activation under stimulating conditions (48) (Figure 5, I and J) and their activities in vivo (45, 67–70), similarly to our *Mef2d*$^{-/-}$ mice. MEF2D functions in Tregs are not limited to the maintenance of a suppressive phenotype, as the proliferation of *Mef2d*$^{-/-}$ Tregs was also impaired, similarly to *Icos*$^{-/-}$ Tregs (71). Moreover, there is indirect evidence of the involvement of MEF2D

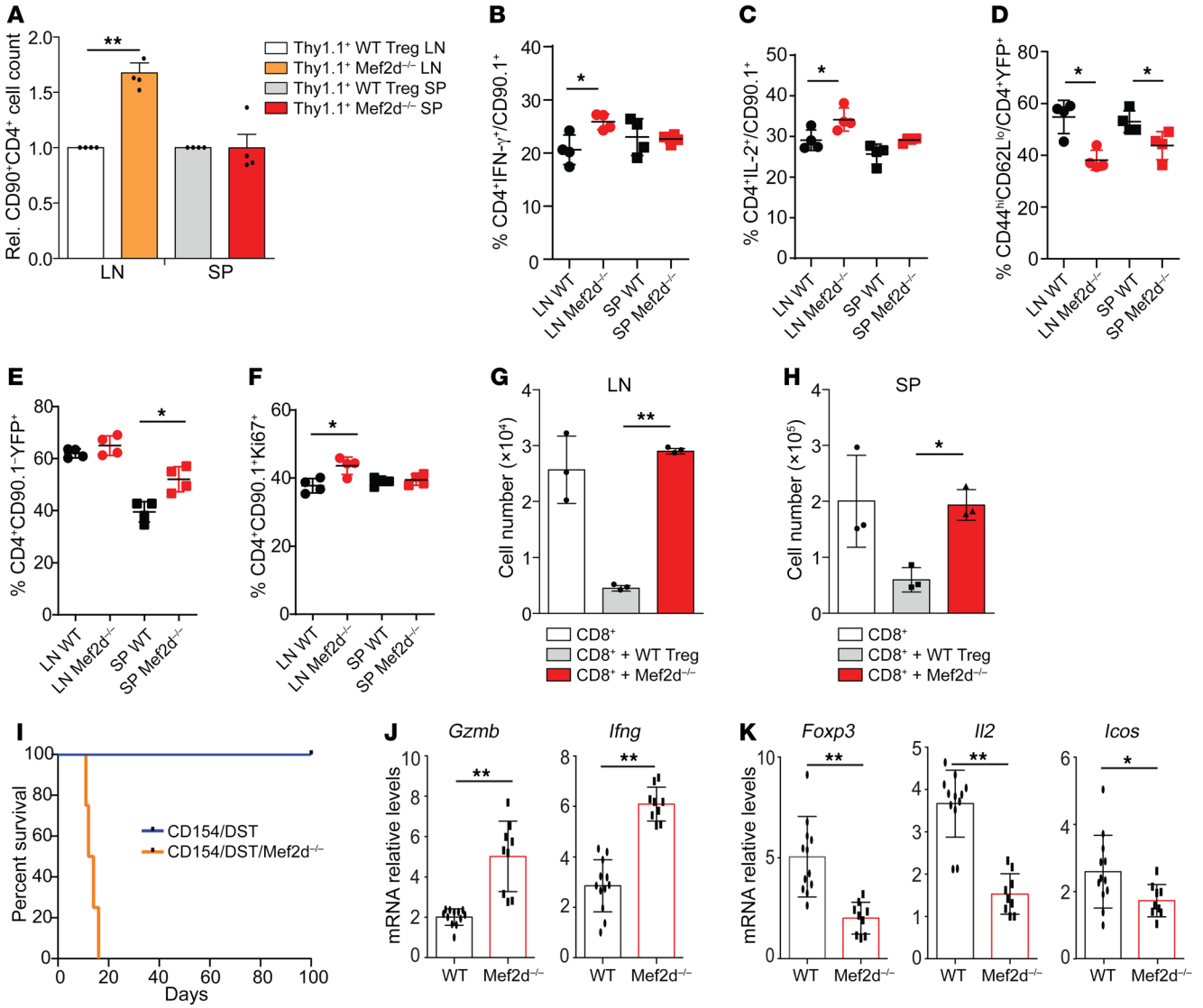

Figure 7. *Mef2d*$^{-/-}$ Treg functions are severely impaired in vivo. (**A**) Twenty-eight days after the adoptive transfer of 0.25 × 10^6 WT Thy1.1$^+$ Teffs and 1.0 × 10^6 WT or *Mef2d*$^{-/-}$ Thy1.2$^+$ Tregs into *Rag1*$^{-/-}$ mice, splenocytes and lymphocytes were harvested and the total number of Thy1.1$^+$ cells determined by flow cytometry; $n = 4$. $^{**}P < 0.01$ by t test. (**B**, **C**, and **F**) Analysis of CD4$^+$Thy1.1$^+$IFN-γ$^+$ (**B**) or IL-2$^+$ (**C**) or Ki67$^+$ (**F**) populations in lymphoid tissues from the same mice as described in **A** stimulated with PMA/ionomycin for 4 hours; $n = 4$. $^*P < 0.05$ by t test. (**D** and **E**) Analysis of CD4$^+$YFP$^+$ (**D**) and CD4$^+$YFP$^+$CD44^{hi} CD62L^{lo} Treg populations (**E**) in lymphoid tissues from the same mice as described in **A**. $^*P < 0.05$ by t test. (**G** and **H**) Twenty-eight days after the adoptive transfer of 0.25 × 10^6 WT Thy1.1$^+$ Teffs and 1.0 × 10^6 WT or *Mef2d*$^{-/-}$ Thy1.2$^+$ Tregs into *Rag1*$^{-/-}$ mice, lymphocytes (**G**) and splenocytes (**H**) were harvested and the total number of Thy1.1$^+$ cells determined by flow cytometry; $n = 4$. $^*P < 0.05$, $^{**}P < 0.01$ by Tukey's multiple-comparison test. (**I**) In contrast to WT recipients, mice with conditional deletion of *Mef2d* in their Foxp3$^+$ Treg cells acutely rejected cardiac allografts (BALB/c→C57BL/6) despite costimulation blockade with anti-CD154 mAb/donor splenocyte transfusion (DST); $n = 5$/group. $P < 0.01$ by Tukey's multiple-comparison test. (**J** and **K**) qPCR results of the expression of the indicated genes in samples collected 2 weeks after cardiac allografting in WT and *Mef2d*$^{-/-}$ mice. $n = 12$ and 9, respectively, for WT and *Mef2d*$^{-/-}$. $^*P < 0.05$, $^{**}P < 0.01$ by t test.

in the regulation of Treg metabolism (31). Finally, and again similarly to CTLA4 (18) and Blimp1 (19), the depletion of MEF2D in Foxp3$^+$ cells affects Tfr functions and impacts the normal maturation of B lymphocytes and the development of GC reactions. As a result of these alterations (50), *Mef2d*$^{-/-}$ mice accumulate small quantities of autoantibodies, though not sufficient to induce significant autoimmunity. It is currently unknown whether the unbalanced B cell homeostasis observed in *Mef2d*$^{-/-}$ mice may actively contribute to anticancer immunity. Further studies are required to clarify this point.

There are no reports in the literature regarding the association of autoimmunity and MEF2D copy-number loss or genetic deletion, probably because of MEF2D pleiotropy. However, a rare SNP that abrogates the expression of the α2 isoform of MEF2D was recently associated with systemic lupus erythematosus (72), and SNPs associated with multiple sclerosis at the level of enhancer and superenhancers were predicted to alter the binding of MEF2 transcription factors (73). Further investigations are required to unveil a likely direct role played by MEF2 transcription factors in these diseases, given our discoveries in Tregs. Finally, our work underlines

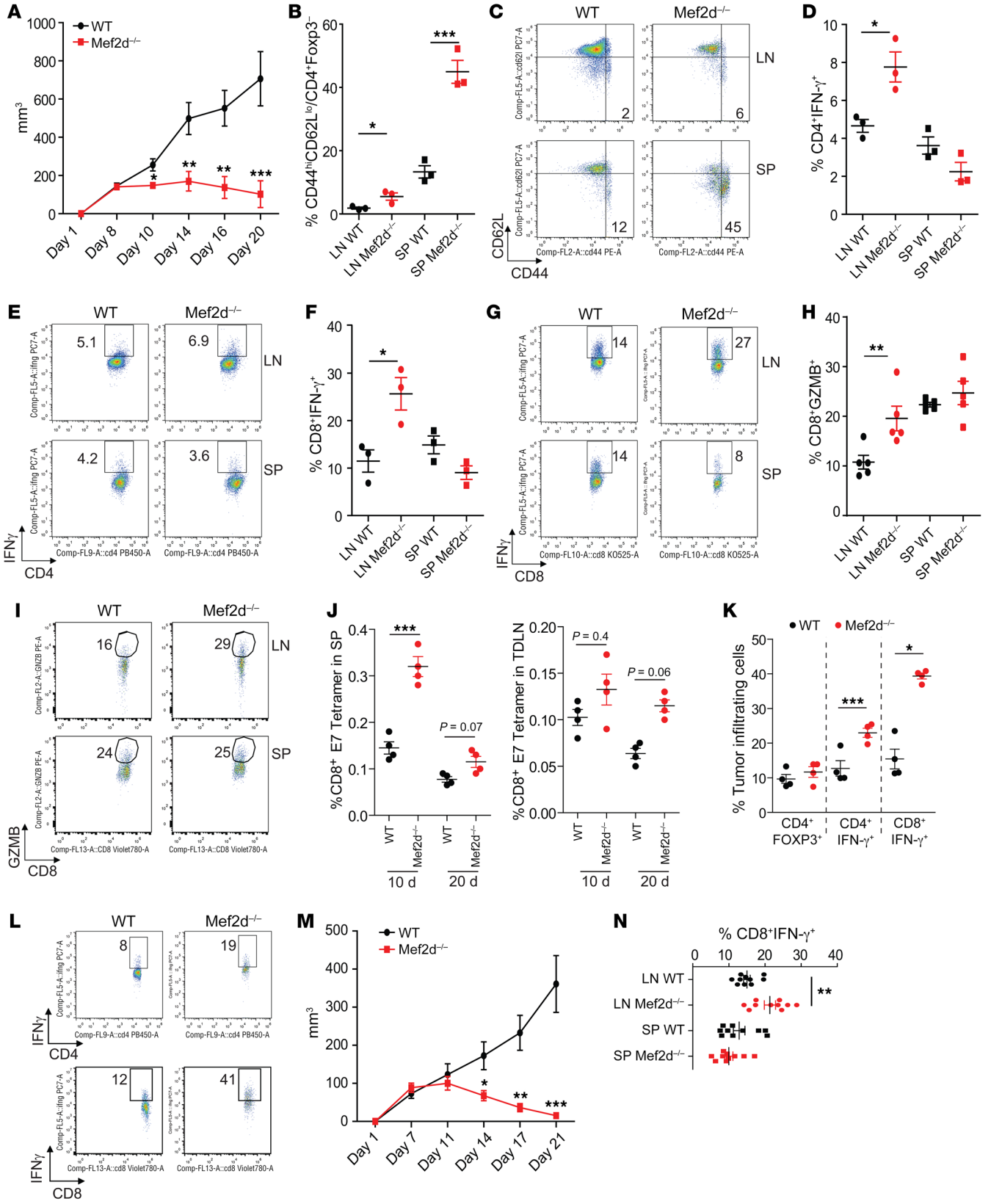
A
WT
Mef2d−/−
mm3
Day 1
Day 8
Day 10
Day 14
Day 16
Day 20
B
% CD44hiCD62Llo/CD4+Foxp3−
LN WT
LN Mef2d−/−
SP WT
SP Mef2d−/−
C
WT
Mef2d−/−
LN
SP
CD62L
CD44
D
% CD4+IFN-γ+
E
IFNγ
CD4
F
% CD8+IFN-γ+
G
CD8
H
% CD8+GZMB+
I
GZMB
J
% CD8+ E7 Tetramer in SP
% CD8+ E7 Tetramer in TDLN
P = 0.07
P = 0.4
P = 0.06
10 d
20 d
K
% Tumor infiltrating cells
CD4+ FOXP3+
CD4+ IFN-γ+
CD8+ IFN-γ+
L
M
N
% CD8+IFN-γ+

Figure 8. *Mef2d* deletion promotes anticancer immunity in mice bearing subcutaneous lung cancers. (**A**) Graphs representing the tumor growth (volume) in 10 WT and 10 *Mef2d*$^{-/-}$ mice during a period of 20 days after the subcutaneous injection of 1.2 × 10^6 TC1 cells. The experiment was repeated twice with similar results (*t* test between the 2 groups for each time point). (**B** and **C**) Analysis of the activation status of CD4$^+$Foxp3$^-$ populations in the same samples as **A**. (**D**–**I**) Analysis of CD4$^+$Foxp3$^-$IFN-γ$^+$ (**D** and **E**), CD8$^+$IFN-γ$^+$ (**F** and **G**), and CD8$^+$GZMB$^+$ (**H** and **I**) populations in single-cell suspensions obtained from the draining lymph nodes and spleens harvested from 3 representative mice injected as in **A** and stimulated for 4 hours with PMA/ionomycin. *n* = 3–5, *t* test. (**J**) CD8 HPV-TC1–specific tetramer staining (E7) positivity in spleens (SP) and tumor-draining lymph nodes (TDLN) of WT and *Mef2d*$^{-/-}$ mice analyzed 10 and 20 days after TC1 cell injection. ***$P < 0.001$ by *t* test. (**K** and **L**) Analysis of tumor-infiltrating CD4$^+$Foxp3$^+$ (**K**) or CD4$^+$IFN-γ$^+$ (**K** and **L**) or CD8$^+$IFN-γ$^+$ (**K** and **L**) populations in tumors harvested from 4 mice per group 8 days after the injection of TC1 cells as in **A**. *n* = 4, *t* test. (**M**) Graphs representing the tumor growth (volume) in 10 WT and 10 *Mef2d*$^{-/-}$ mice during a period of 21 days after the subcutaneous injection of 2.0 × 10^5 AE.17 cells, *t* test. (**N**) Analysis of CD8$^+$IFN-γ$^+$ populations in single-cell suspensions obtained from the draining lymph nodes and spleens harvested from mice injected with AE.17 cells (*n* = 10, *t* test). *$P < 0.05$, **$P < 0.01$, ***$P < 0.005$.

the importance played by MEF2D in the regulation of anticancer immunity, offering an alternative interpretation of the conflicting evidence about the contribution of MEF2D to oncogenesis (41).

Methods

Mice. We used BALB/c, *Rag1*$^{-/-}$ C57BL/6, and CD90.1/B6 mice from The Jackson Laboratory, plus previously described *Foxp3*$^{YFP\text{-}Cre}$ mice (68) and *Mef2d*$^{fl/fl}$ mice (40) that were backcrossed on the C57BL/6 background at least 8 times and used at 6–8 weeks of age, unless specified otherwise. *Foxp3*$^{YFP\text{-}Cre}$ mice were used as WT controls.

Plasmids and transfections. We purchased Mef2d-FLAG-MYC plasmids from Origene and FLAG-tagged Foxp3 from Addgene. MEF2D-GFP and MEF2D deletion mutants were previously described (38). Hdac9-FLAG was obtained from Ed Seto (George Washington University, Washington, DC) (74). MEF2Dα1 and MEF2Dα2 were obtained from F. Jeffrey Dilworth (Ottawa Hospital Research Institute, Ottawa, Canada) (36). HEK293T cells were grown in DMEM plus 10% FBS and transfected with Lipofectamine 2000 (Invitrogen, 11668027).

Co-IP and Western blotting. HEK293T, Teff, and Treg cells were lysed with a hypotonic buffer (20 mM Tris-HCl, pH 7.5; 2 mM EDTA; 10 mM $MgCl_2$; 10 mM KCl; and 1% Triton X-100) supplemented with protease inhibitors. For each immunoprecipitation, 1 μg of Ab was used. Ab-antigen complexes were collected with Protein G agarose (Invitrogen, 15920-010). Cell lysates were resolved by SDS-PAGE, transferred to nitrocellulose membranes, and immunoblotted with the following Abs: MEF2D (BD, 610774), Foxp3 (Invitrogen, 700914; eBioscience, 14-4774-82, 13-5773-80), p300 (Invitrogen, PA1-848), FLAG (Cell Signaling Technology [CST], 14793), Myc (CST, 2272), HA (CST, 2367), phospho-histone H2A.X (Ser139; CST, 9718), histone H2A.X (CST, 7631), p53 mAb (DO-1; CST, 18032), β-actin (CST, 3700), Blimp1 (eBioscience, 6D3, 14-5963-82), Hdac3 (Abcam, ab7030), Crabp2 (Santa Cruz Biotechnology, sc-166897), Fabp5 (Santa Cruz Biotechnology, sc-365236), Lmnb1 (Santa Cruz Biotechnology, sc-377000), Ki67 (Abcam, ab15580), p53ac (K120) (Abcam, 78316), and MEF2D (α1 and α2) (36). Secondary HRP-conjugated Abs against mouse (catalog 7076), rat (catalog 7077), and rabbit (catalog 7074) IgG were purchased from CST. Unconjugated anti-CD3 (clone 145-2C11, 553057) and anti-CD28 (clone 37.51, 553294) mAbs used for cell activation were purchased from BD.

Cryopreservation. Single-cell suspensions in CryoStor CS5 cryopreservation media (MilliporeSigma) reagent were frozen at –80°C, stored in liquid nitrogen, and then thawed and transferred quickly into greater than 10 volumes of warm tissue culture medium (DMEM, Thermo Fisher Scientific) for use. Cell number and viability were assessed with a Nexcelom Cellometer Auto2000 and AOPI Staining solution in PBS.

Flow cytometry. Single-cell suspensions from lymph nodes, spleens, or tumors were prepared as previously described (75) and were stained with fluorochrome-conjugated mAbs from BD Biosciences, unless specified otherwise, that were directed against CD4 (Pacific Blue, Invitrogen, MHCD0428), CD8 (Super Bright 645, eBioscience, clone 53-6.7, 64-0081-82), Foxp3 (eFluor 450, eBioscience, clone FJK-16s, 48-5773-82 and PE-Cy5, 15-5773-82), CD62L (PE-Cy7, clone MEL-14, 25-0621-82), IFN-γ (APC, clone XMG1.2, 554413; PE 554412), CD44 (PE-Cyanine5, eBioscience, clone IM7, 15-0441-83), CTLA4 (APC, 17-1522-82), Icos (PE, 12-9949-81), Ki67 (APC700, 561277), IL-2 (PE, eBioscience, clone JES6-5H4, 12-7021-41), CD25 (APC, eBioscience, clone PC61.5, 17-0251-82), CD8a (FITC, 53-6.7), CD4 (FITC, H129.19), NK1.1 (FITC, M1/70, BioLegend), CD11b (FITC, M1/70, BioLegend), CD19 (BV605, 6D5, BioLegend), CD45R/B220 (BV785, RA3-6B2, BioLegend), IgM (PerCP-Cy5.5, II-41, Invitrogen), CD62L (PE, MEL-14, BioLegend), CD95 (PE-CF594, Jo2), GL7 (APC, GL7, BioLegend), CD138 (APC-R700, 281-2), CD93 (PE/Cy7, AA4.1, BioLegend), CD23 (APC Cy7, B3B4, BioLegend), CD21/35 (PB, 7E9, BioLegend), CD19 (FITC, 6D5, BioLegend), CD4 (PE-CF594, RM4-5), CXCR5 (APC, L138D7, BioLegend), PD-1 (PE/Cy7, 29F.1A12, BioLegend), and Foxp3 (PB, FJK-16s, Invitrogen) and acquired on a Cytoflex (Beckman Coulter) flow cytometer.

Treg suppression assays. For in vitro studies, 5 × 10^4 CD4$^+$CD25$^-$YFP$^-$ T cells and CD4$^+$CD25$^+$YFP$^+$ Tregs from *Foxp3*$^{YFP\text{-}Cre}$ and *Mef2d*$^{-/-}$ mice isolated using a CD4$^+$CD25$^+$ Treg isolation kit (Miltenyi Biotec, 130-091-041) or cell sorted were added to 96-well plates. Equal numbers of CFSE-labeled CD4$^+$CD25$^-$ T cells and γ-irradiated antigen-presenting cells, isolated using a CD90.1 kit (Miltenyi Biotec, 130-049-101), plus anti-CD3 mAb (1 μg/mL), were cultured for 72 hours. After 72 hours, proliferation of Teff cells was determined by flow and analysis of CellTrace Violet (Thermo Fisher Scientific) dilution. The same assay was performed by using Tregs isolated from mice treated with IL-2/anti–IL-2 complexes (76), or by preactivating Tregs for 2 days with anti-CD3/anti-CD28 beads (1:1) and IL-2 (10 U/mL) (48). For Treg assay performed by using WT splenocytes as responder cells, WT splenocytes were CFSE labeled and cultured in the presence of WT and *Mef2d*$^{-/-}$ Tregs for 3 days under CD3 stimulation (anti-CD3 mAb, 1 μg/mL).

For in vivo homeostatic proliferation assay, 0.2 × 10^6 CD4$^+$CD25$^-$Thy1.1$^+$ or 0.2 × 10^6 CD8$^+$Thy1.1$^+$ and 1.0 × 10^6 Tregs were injected via the tail vein into *Rag1*$^{-/-}$ mice. After 1 or 4 weeks, lymph nodes and spleens were harvested and stained with Thy1.1-PE and CD4–Pacific Blue or CD8–Super Bright 645, and the numbers of Thy1.1$^+$ T cells determined using a Cytoflex flow cytometer.

Cardiac transplantation. Heterotopic cardiac allografts were performed using BALB/c donors and WT or *Mef2d*$^{-/-}$ recipients on the

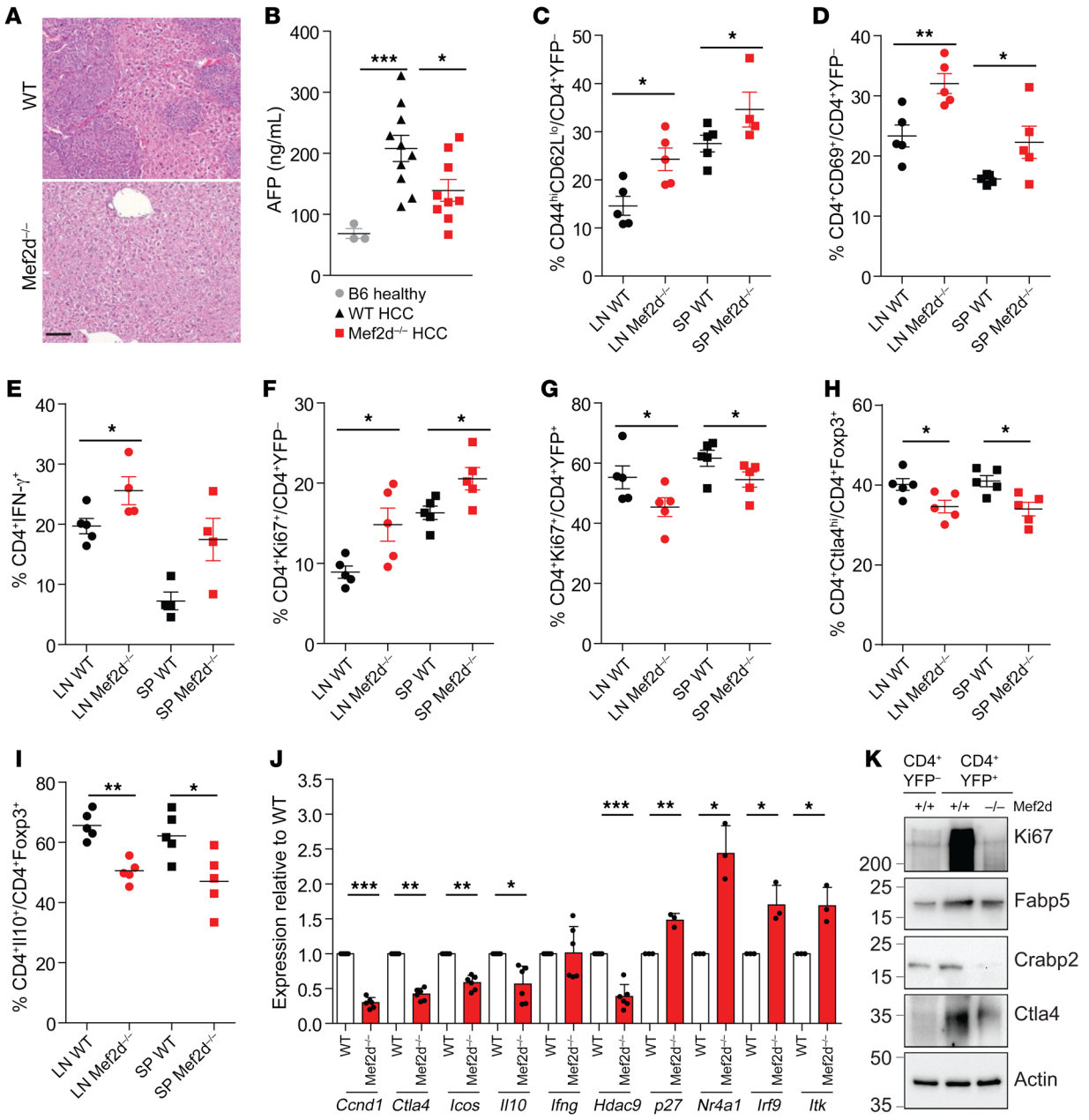

Figure 9. *Mef2d* deletion promotes anticancer immunity in mice bearing HCC. Shown is the analysis on day 9 after tumor cell injections, and additional data at 21 days after injection are shown in Supplemental Figure 11. (**A**) H&E-stained sections of WT and *Mef2d*$^{-/-}$ livers 9 days after the injection of 0.3 × 10^6 HCC cells into the mesenteric vein. Scale bar: 100 μm. Livers from WT show dense tumors, whereas livers from *Mef2d*$^{-/-}$ mice are tumor free. (**B**) Dot plot representing the AFP serum levels of 3 healthy C57BL/6 mice and 10 WT and 10 *Mef2d*$^{-/-}$ mice on day 9 after HCC injection; Tukey's multiple-comparison test. (**C**–**F**) Analysis of the activation status of CD4$^+$Foxp3$^-$ and CD8$^+$ populations in terms of CD44^{hi}CD62L^{lo} (**C**), CD69 (**D**), and Ki67 positivity (**F**) and production of IFN-γ (**E**) in freshly isolated (**C**, **D**, and **F**) or PMA/ionomycin-stimulated (**E**) cells obtained from lymphoid tissues of HCC-injected mice. *n* = 5, *t* test. (**G**–**I**) Analysis of the expression of Ki67 (**G**), CTLA4 (**H**), and IL-10 (**I**) in CD4$^+$Foxp3$^+$ populations in freshly isolated (**G**) or PMA/ionomycin-stimulated (**H** and **I**) single-cell suspensions obtained from the same samples used for **C**. *n* = 5, *t* test. (**J**) qPCR results of the expression of the indicated genes in YFP$^+$ Tregs obtained from the draining lymph nodes of WT and *Mef2d*$^{-/-}$ HCC-injected mice; *n* = 3–5, *t* test. (**K**) Immunoblots of Ki67, Crabp2, Fabp5, and CTLA4 in the same cells described in Figure 9J; β-actin served as loading control. *P < 0.05; **P < 0.01; ***P < 0.005.

C57BL/6 background (77). At the time of engraftment, recipients were treated i.v. with anti-CD154 mAb (200 μg) plus 5 × 10^6 donor splenocytes (49). Allograft survival was monitored by palpation of ventricular contractions and confirmed by histological evaluation.

Detection of autoantibodies. Sera of 3 WT and *Mef2d*$^{-/-}$ mice were tested for autoantibodies by indirect immunofluorescence. Nonfixed 4- to 5-μm cryosections of WT tissues were incubated for 1 hour at room temperature with serial dilutions (from 1:1 up to 1:80) of sera, washed in PBS, and incubated for 30 minutes at room temperature with FITC-labeled goat anti-mouse secondary Ab (Jackson Immunoresearch Lab, 115-545-062; diluted in PBS, 1:200). After washings in PBS, slides were mounted and evaluated by specialist in autoim-

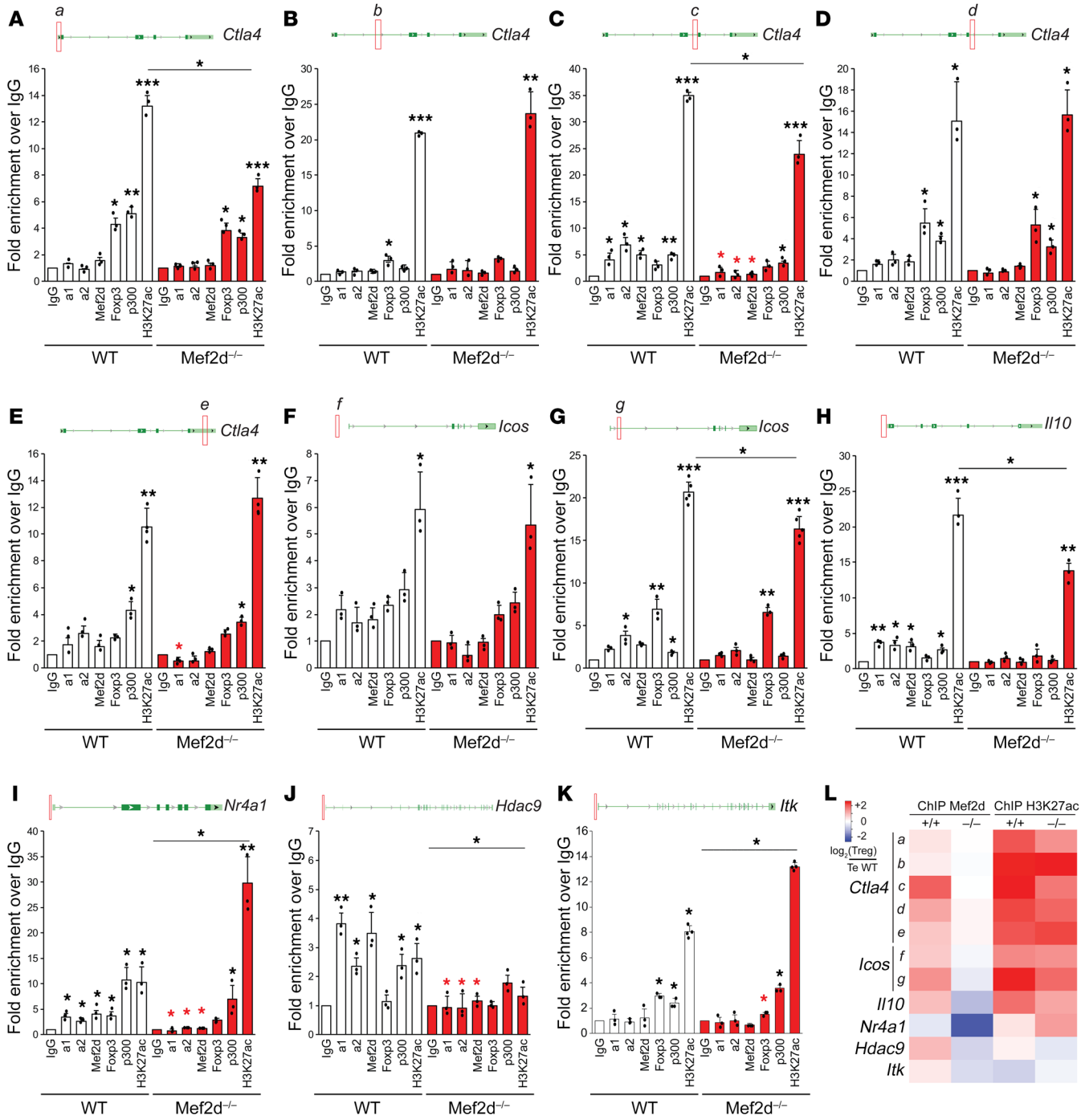

Figure 10. MEF2D works synergistically, additively, and independently from Foxp3 in regulating the expression of the bound loci. (**A**–**K**) Histogram representing the qPCR results obtained in freshly isolated WT and *Mef2d*$^{-/-}$ Tregs after ChIP with the indicated Abs. For each investigated genomic locus, a red square indicates the position of the amplified region with respect to the leading TSS and the exons of the associated canonical mRNA isoform (n = 2–5). Black asterisks indicate the significance of the indicated comparisons or with respect to IgG, and red asterisks the significance of the comparison of the same IP between WT and *Mef2d*$^{-/-}$ Tregs. *$P < 0.05$; **$P < 0.01$; ***$P < 0.005$ by t test and Tukey's multiple-comparison test. (**L**) Heatmap representing the strength of MEF2D and H3K27ac signals for each genomic locus in WT and *Mef2d*$^{-/-}$ Tregs with respect to WT Teffs.

mune clinical diagnostics in human autoimmune diseases. Precharacterized sera from mice with known autoantibodies of corresponding specificity were used as positive controls, while pooled sera from WT B6 mice and secondary Abs only were used as negative controls. All positive sera were analyzed a second time to evaluate individual titers.

Immunoperoxidase. Formalin-fixed, paraffin-embedded sections of allografts harvested at 14 days post-Tx were stained by immunoperoxidase with rabbit Abs directed against CD3 (A0452, Agilent), C4d (12-5000, American Research Products), or rabbit IgG control Ab (I-1000, Vector Labs) (49).

Table 2. Primers used in this study

Primer name	Sequence 5′→3′
ITK_+34_FW	GTGCGACTGAAGGAGAGGAG
Itk_-107_RV	CATCAGAGGAGGGAGCTCAG
Nr4a1_-357_FW	CCTCCTCCTGGTCGGTTATT
Nr4a1_-219_RV	GCGCGGATTGTTTGATCTAT
Hdac9_-482_FW	CTCCAGAGGGTGTCCTCCTA
Hdac9_-710_RV	GGCTTTGGTGGGGTATTTTT
Ctla4_+4397_FW	AAGGAGCAGGAAGGATAGGG
Ctla4_+4584_RV	GCTGCTCCATGTTGTTCAAA
Ctla4_+4003_fw	CTTGTCCCTTTGATGGCACT
Ctla4_+4200_rv	TGGATCTGCAACAGAAGACG
Ctla4_-210_fw	CTCCAAGACTCCACGTCTCC
Ctla4_+15_rv	AGCCGTGGGTTTAGCTGTTA
Ctla4_+1959_fw	CCCGCTAAGCTGATGGAGTA
Ctla4_+2199_rv	TACCCCAGGCTTAGTTTCCA
Ctla4_+6339_fw	AATCCATCAGGTTGGACTCG
Ctla4_+6524_rv	AACACTGCCAGCTTTTGGTT
Icos_-2490_fw	CCTCAGTCAGAAGGGTCGTC
Icos_-2324_rv	CAGAAATTCCTGGTCATGTTTT
Icos_+605_fw	AGTCTGCCATAGGGTTGGTG
Icos_+769_rv	TCAGTCATTTTCTCCCCCTTT
Il10_-172_fw	TCTTTAGCGCTTACAATGCAAA
Il10_-10_rv	CTGTTCTTGGTCCCCCTTTT
Itk_rt_fw	GCATCCCGTGCCACTATAAAT
Itk_rt_rv	CTGCCGACTCTCACAGTCTG
Irf9_rt_fw	CCTCAGGCAAAGTACGCTG
Irf9_rt_rv	GGGGTGTCCTATGTCCCCA
Mef2d_pan_rt_fw	CCCGTTGGGAATGGCTATGT
Mef2d_pan_rt_rv	TTAACCCTTTGCCTCCCTGG
Mef2da1_fw_rt	AGCTGGATGGGCTCTTCAG
Mef2da1_rv_rt	CAGCATGGCTCCTGCACTA
Mef2da2_fw_rt	CCAGACGGAAGAGAAGTAT
Mef2da2_rv_rt	TGACATAGCCATTCCCAACG

ChIP assays. Teffs or Tregs were fixed for 15 minutes with 1% formaldehyde and fragmented by sonication. Chromatin was immunoprecipitated as previously described (38) using Abs against H3K27ac (2 μg, Abcam, ab4729), MEF2D (5 μg, BD, 610774), MEF2Dα1 and MEF2Dα2 (36) (5 μg), p300 (3 μg, Invitrogen, PA1-848), and Foxp3 (10 μg, Invitrogen, PA1-806). The immunoprecipitated DNA was purified and analyzed by qPCR (SYBR Green, Applied Biosystems).

RNA-seq and real-time qPCR. RNA was isolated using RNeasy kits (QIAGEN), and RNA integrity and quantity were analyzed by NanoDrop ND-1000 and Nanochip 2100 Bioanalyzer (Agilent Technologies). Library preparation, RNA-seq, genome mapping, and analysis were performed by Novogene on the Illumina Platform PE150; data were deposited in the NCBI's Gene Expression Omnibus (GEO) database (accession GSE139480). The edgeR package (https://bioconductor.org/packages/release/bioc/html/edgeR.html) was used to identify the differentially expressed genes (P value < 0.05 and fold change > 1.3). GSEA (78) was performed to identify altered signaling pathways, as previously described (38). Expression of individual genes was verified by qPCR. RNA was reverse transcribed to cDNA (Applied Biosystems) and RT-qPCR was performed using TaqMan primer and probe sets; data were normalized to endogenous *18S* rRNA, and relative expression was determined by the formula $2^{-\Delta CT}$.

Cell lines and tumor models. The murine lung adenocarcinoma cells, TC1 (79), were provided by Yvonne Paterson (University of Pennsylvania). The murine AE17.ova mesothelioma cell line (80) was provided by Delia Nelson, University of Western Australia, Perth, Australia. The murine HCC cell line, Dt81-Hepa1-6, was developed by Marc Bilodeau (Centre Hospitalier de l'Université de Montréal, Montreal, Canada) (81). Lung cancer cells were grown in RPMI, and HCC cells were grown in DMEM/F-12 supplemented with 10% FBS, 2 mM glutamine, and 5 μg/mL penicillin/streptomycin. For lung tumor cells, each mouse was shaved on their right flank and injected s.c. with 1.2×10^6 TC1 or 2×10^6 AE17 tumor cells, whereas 0.3×10^6 HCC cells were injected directly into the mesenteric vein. Tumor volume was determined by the formula $V = (W^2 \times L)/2$. Serum AFP was measured by using a mouse alpha-Fetoprotein/AFP Quantikine ELISA Kit (MAFP00, R&D Systems).

Statistics. Data were analyzed using GraphPad Prism 8.0. Data are presented as mean ± SD unless specified otherwise. Measurements between 2 groups were done with a 2-tailed Student's t test if data were normally distributed or unpaired Mann-Whitney U test when the populations were not normally distributed. Comparison of multiple samples was performed by 1-way ANOVA with corresponding Tukey's multiple-comparison test. Graft survival was evaluated with Kaplan-Meier followed by log-rank test. AUC for suppression assays was calculated as previously described (82); AUC for KO samples was expressed as ratio to WT, then ratios of 3 experiments were combined and tested for significance (1-sample t test with theoretical mean = 1). P less than 0.05 was considered significant: $^*P < 0.05$, $^{**}P < 0.01$, $^{***}P < 0.005$.

Study approval. Animal studies were approved by the Institutional Animal Care and Use Committee of the Children's Hospital of Philadelphia (protocols 17-001047 and 19-000561).

Primers. The primers used are listed in Table 2.

Author contributions

EDG contributed important Mef2 expertise, designed and performed experiments, analyzed data, and drafted the manuscript. LW performed cardiac allografts, performed experiments, and analyzed data. YX performed experiments and analyzed data. TA performed experiments and analyzed data. LMC performed experiments and analyzed data. RH provided technical assistance. AS performed experiments. TRB performed experiments. MT provided technical support. UHB provided assistance with RNA-seq studies. WWH oversaw experimental design and writing of the manuscript.

Acknowledgments

This work was supported by NIH grants R01 AI12324 and R01 CA177852 (to WWH). EDG received a "Fondazione Umberto Veronesi Fellowship." Specified plasmids were purchased from Addgene. We acknowledge the gifts of reagents and cells from F. Jeffrey Dilworth (Ottawa, Canada) and from Marc Bilodeau (Montreal, Canada), respectively.

Address correspondence to: Wayne W. Hancock, Children's Hospital of Philadelphia, 916B Abramson Research Center, 3615 Civic Center Boulevard, Philadelphia, Pennsylvania 19104, USA. Phone: 215.590.8709; Email: whancock@pennmedicine.upenn.edu.

1. Sakaguchi S, Miyara M, Costantino CM, Hafler DA. FOXP3+ regulatory T cells in the human immune system. *Nat Rev Immunol*. 2010;10(7):490–500.
2. Tanaka A, Sakaguchi S. Regulatory T cells in cancer immunotherapy. *Cell Res*. 2017;27(1):109–118.
3. Rudensky AY. Regulatory T cells and Foxp3. *Immunol Rev*. 2011;241(1):260–268.
4. Samstein RM, et al. Foxp3 exploits a pre-existent enhancer landscape for regulatory T cell lineage specification. *Cell*. 2012;151(1):153–166.
5. Chorro L, et al. Interleukin 2 modulates thymic-derived regulatory T cell epigenetic landscape. *Nat Commun*. 2018;9(1):5368.
6. Ren J, et al. Foxp1 is critical for the maintenance of regulatory T-cell homeostasis and suppressive function. *PLoS Biol*. 2019;17(5):e3000270.
7. Li B, et al. FOXP3 is a homo-oligomer and a component of a supramolecular regulatory complex disabled in the human XLAAD/IPEX autoimmune disease. *Int Immunol*. 2007;19(7):825–835.
8. van Loosdregt J, et al. Regulation of Treg functionality by acetylation-mediated Foxp3 protein stabilization. *Blood*. 2010;115(5):965–974.
9. Beier UH, et al. Sirtuin-1 targeting promotes Foxp3+ T-regulatory cell function and prolongs allograft survival. *Mol Cell Biol*. 2011;31(5):1022–1029.
10. Huang C, et al. Cutting Edge: a novel, human-specific interacting protein couples FOXP3 to a chromatin-remodeling complex that contains KAP1/TRIM28. *J Immunol*. 2013;190(9):4470–4473.
11. Wang L, et al. Histone/protein deacetylase inhibitor therapy for enhancement of Foxp3+ T-regulatory cell function posttransplantation. *Am J Transplant*. 2018;18(7):1596–1603.
12. Tanaka S, Pfleger C, Lai JF, Roan F, Sun SC, Ziegler SF. KAP1 regulates regulatory T cell function and proliferation in both Foxp3-dependent and -independent manners. *Cell Rep*. 2018;23(3):796–807.
13. Huang J, et al. Histone/protein deacetylase 11 targeting promotes Foxp3+ Treg function. *Sci Rep*. 2017;7(1):8626.
14. Lee S, Park K, Kim J, Min H, Seong RH. Foxp3 expression in induced regulatory T cells is stabilized by C/EBP in inflammatory environments. *EMBO Rep*. 2018;19(12):e45995.
15. Carpenter AC, et al. Control of regulatory T cell differentiation by the transcription factors Thpok and LRF. *J Immunol*. 2017;199(5):1716–1728.
16. Ohnmacht C, et al. Mucosal immunology. The microbiota regulates type 2 immunity through RORγt+ T cells. *Science*. 2015;349(6251):989–993.
17. Sefik E, et al. Mucosal immunology. Individual intestinal symbionts induce a distinct population of RORγ+ regulatory T cells. *Science*. 2015;349(6251):993–997.
18. Chung Y, et al. Follicular regulatory T cells expressing Foxp3 and Bcl-6 suppress germinal center reactions. *Nat Med*. 2011;17(8):983–988.
19. Linterman MA, et al. Foxp3+ follicular regulatory T cells control the germinal center response. *Nat Med*. 2011;17(8):975–982.
20. Fang D, Zhu J. Dynamic balance between master transcription factors determines the fates and functions of CD4 T cell and innate lymphoid cell subsets. *J Exp Med*. 2017;214(7):1861–1876.
21. Cretney E, et al. The transcription factors Blimp-1 and IRF4 jointly control the differentiation and function of effector regulatory T cells. *Nat Immunol*. 2011;12(4):304–311.
22. Potthoff MJ, Olson EN. MEF2: a central regulator of diverse developmental programs. *Development*. 2007;134(23):4131–4140.
23. Ma K, Chan JK, Zhu G, Wu Z. Myocyte enhancer factor 2 acetylation by p300 enhances its DNA binding activity, transcriptional activity, and myogenic differentiation. *Mol Cell Biol*. 2005;25(9):3575–3582.
24. Miska EA, Karlsson C, Langley E, Nielsen SJ, Pines J, Kouzarides T. HDAC4 deacetylase associates with and represses the MEF2 transcription factor. *EMBO J*. 1999;18(18):5099–5107.
25. Swanson BJ, Jack HM, Lyons GE. Characterization of myocyte enhancer factor 2 (MEF2) expression in B and T cells MEF2C is a B cell-restricted transcription factor in lymphocytes. *Mol Immunol*. 1998;35(8):445–458.
26. Pan F, Ye Z, Cheng L, Liu JO. Myocyte enhancer factor 2 mediates calcium-dependent transcription of the interleukin-2 gene in T lymphocytes: a calcium signaling module that is distinct from but collaborates with the nuclear factor of activated T cells (NFAT). *J Biol Chem*. 2004;279(15):14477–14480.
27. Matsuoka H, et al. Disruption of HDAC4/N-CoR complex by histone deacetylase inhibitors leads to inhibition of IL-2 gene expression. *Biochem Pharmacol*. 2007;74(3):465–476.
28. Esau C, Boes M, Youn HD, Tatterson L, Liu JO, Chen J. Deletion of calcineurin and myocyte enhancer factor 2 (MEF2) binding domain of Cabin1 results in enhanced cytokine gene expression in T cells. *J Exp Med*. 2001;194(10):1449–1459.
29. Dequiedt F, et al. HDAC7, a thymus-specific class II histone deacetylase, regulates Nur77 transcription and TCR-mediated apoptosis. *Immunity*. 2003;18(5):687–698.
30. Tao R, et al. Deacetylase inhibition promotes the generation and function of regulatory T cells. *Nat Med*. 2007;13(11):1299–1307.
31. Beier UH, et al. Essential role of mitochondrial energy metabolism in Foxp3+ T-regulatory cell function and allograft survival. *FASEB J*. 2015;29(6):2315–2326.
32. Kasler HG, Lim HW, Mottet D, Collins AM, Lee IS, Verdin E. Nuclear export of histone deacetylase 7 during thymic selection is required for immune self-tolerance. *EMBO J*. 2012;31(23):4453–4465.
33. Hakim NH, Kounishi T, Alam AH, Tsukahara T, Suzuki H. Alternative splicing of Mef2c promoted by Fox-1 during neural differentiation in P19 cells. *Genes Cells*. 2010;15(3):255–267.
34. Di Giorgio E, Gagliostro E, Clocchiatti A, Brancolini C. The control operated by the cell cycle machinery on MEF2 stability contributes to the downregulation of CDKN1A and entry into S phase. *Mol Cell Biol*. 2015;35(9):1633–1647.
35. Martin JF, Miano JM, Hustad CM, Copeland NG, Jenkins NA, Olson EN. A Mef2 gene that generates a muscle-specific isoform via alternative mRNA splicing. *Mol Cell Biol*. 1994;14(3):1647–1656.
36. Sebastian S, et al. Tissue-specific splicing of a ubiquitously expressed transcription factor is essential for muscle differentiation. *Genes Dev*. 2013;27(11):1247–1259.
37. Gao C, et al. RBFox1-mediated RNA splicing regulates cardiac hypertrophy and heart failure. *J Clin Invest*. 2016;126(1):195–206.
38. Di Giorgio E, et al. The co-existence of transcriptional activator and transcriptional repressor MEF2 complexes influences tumor aggressiveness. *PLoS Genet*. 2017;13(4):e1006752.
39. Rudra D, et al. Transcription factor Foxp3 and its protein partners form a complex regulatory network. *Nat Immunol*. 2012;13(10):1010–1019.
40. Kim Y, et al. The MEF2D transcription factor mediates stress-dependent cardiac remodeling in mice. *J Clin Invest*. 2008;118(1):124–132.
41. Di Giorgio E, Hancock WW, Brancolini C. MEF2 and the tumorigenic process, hic sunt leones. *Biochim Biophys Acta Rev Cancer*. 2018;1870(2):261–273.
42. Fu W, et al. A multiply redundant genetic switch 'locks in' the transcriptional signature of regulatory T cells. *Nat Immunol*. 2012;13(10):972–980.
43. Cretney E, Kallies A, Nutt SL. Differentiation and function of Foxp3(+) effector regulatory T cells. *Trends Immunol*. 2013;34(2):74–80.
44. Zheng Y, et al. Regulatory T-cell suppressor program co-opts transcription factor IRF4 to control T(H)2 responses. *Nature*. 2009;458(7236):351–356.
45. Bankoti R, et al. Differential regulation of Effector and Regulatory T cell function by Blimp1. *Sci Rep*. 2017;7(1):12078.
46. Yu J, Angelin-Duclos C, Greenwood J, Liao J, Calame K. Transcriptional repression by blimp-1 (PRDI-BF1) involves recruitment of histone deacetylase. *Mol Cell Biol*. 2000;20(7):2592–2603.
47. Wei X, et al. Reciprocal expression of IL-35 and IL-10 defines two distinct effector Treg subsets that are required for maintenance of immune tolerance. *Cell Rep*. 2017;21(7):1853–1869.
48. Koizumi SI, et al. JunB regulates homeostasis and suppressive functions of effector regulatory T cells. *Nat Commun*. 2018;9(1):5344.
49. Hancock WW, Sayegh MH, Zheng XG, Peach R, Linsley PS, Turka LA. Costimulatory function and expression of CD40 ligand, CD80, and CD86 in vascularized murine cardiac allograft rejection. *Proc Natl Acad Sci U S A*. 1996;93(24):13967–13972.
50. Princler GL, Vlahakis G, Kortright KH, Okada S, McIntire KR. Dynamics of serum alpha-fetoprotein during spontaneous hepatocellular carcinoma development in mice. *Eur J Cancer Clin Oncol*. 1981;17(12):1241–1248.
51. Liopeta K, et al. cAMP regulates IL-10 production by normal human T lymphocytes at multiple levels: a potential role for MEF2. *Mol Immunol*. 2009;46(3):345–354.
52. Boubali S, et al. Calcium/calmodulin-dependent protein kinase II regulates IL-10 production by human T lymphocytes: a distinct target in the calcium dependent pathway. *Mol Immunol*. 2012;52(2):51–60.
53. Yang S, et al. Transcription factor myocyte enhancer factor 2D regulates interleukin-10 production in microglia to protect neuronal cells from inflammation-induced death. *J Neuroinflammation*. 2015;12:33.

54. Youn HD, Liu JO. Cabin1 represses MEF2-dependent Nur77 expression and T cell apoptosis by controlling association of histone deacetylases and acetylases with MEF2. *Immunity*. 2000;13(1):85–94.
55. Daems C, Martin LJ, Brousseau C, Tremblay JJ. MEF2 is restricted to the male gonad and regulates expression of the orphan nuclear receptor NR4A1. *Mol Endocrinol*. 2014;28(6):886–898.
56. Di Giorgio E, et al. MEF2 is a converging hub for histone deacetylase 4 and phosphatidylinositol 3-kinase/Akt-induced transformation. *Mol Cell Biol*. 2013;33(22):4473–4491.
57. Rastogi B, Raut SK, Panda NK, Rattan V, Radotra BD, Khullar M. Overexpression of HDAC9 promotes oral squamous cell carcinoma growth, regulates cell cycle progression, and inhibits apoptosis. *Mol Cell Biochem*. 2016;415(1–2):183–196.
58. Andzelm MM, et al. MEF2D drives photoreceptor development through a genome-wide competition for tissue-specific enhancers. *Neuron*. 2015;86(1):247–263.
59. Cretney E, et al. Characterization of Blimp-1 function in effector regulatory T cells. *J Autoimmun*. 2018;91:73–82.
60. Pedroza-Gonzalez A, et al. Activated tumor-infiltrating $CD4^+$ regulatory T cells restrain antitumor immunity in patients with primary or metastatic liver cancer. *Hepatology*. 2013;57(1):183–194.
61. Liu Y, et al. Inhibition of p300 impairs $Foxp3^+$ T regulatory cell function and promotes antitumor immunity. *Nat Med*. 2013;19(9):1173–1177.
62. Wang L, et al. Ubiquitin-specific protease-7 inhibition impairs Tip60-dependent $Foxp3^+$ T-regulatory cell function and promotes antitumor immunity. *EBioMedicine*. 2016;13:99–112.
63. Ma L, et al. Overexpression of the transcription factor MEF2D in hepatocellular carcinoma sustains malignant character by suppressing G2-M transition genes. *Cancer Res*. 2014;74(5):1452–1462.
64. Song L, et al. miR-218 suppressed the growth of lung carcinoma by reducing MEF2D expression. *Tumour Biol*. 2016;37(3):2891–2900.
65. Jayathilaka N, et al. Inhibition of the function of class IIa HDACs by blocking their interaction with MEF2. *Nucleic Acids Res*. 2012;40(12):5378–5388.
66. Wei J, et al. Reversal of pathological cardiac hypertrophy via the MEF2-coregulator interface. *JCI Insight*. 2017;2(17):e91068.
67. Guo F, Iclozan C, Suh WK, Anasetti C, Yu XZ. CD28 controls differentiation of regulatory T cells from naive CD4 T cells. *J Immunol*. 2008;181(4):2285–2291.
68. Rubtsov YP, et al. Regulatory T cell-derived interleukin-10 limits inflammation at environmental interfaces. *Immunity*. 2008;28(4):546–558.
69. Sojka DK, Hughson A, Fowell DJ. CTLA-4 is required by $CD4^+CD25^+$ Treg to control $CD4^+$ T-cell lymphopenia-induced proliferation. *Eur J Immunol*. 2009;39(6):1544–1551.
70. Paterson AM, et al. Deletion of CTLA-4 on regulatory T cells during adulthood leads to resistance to autoimmunity. *J Exp Med*. 2015;212(10):1603–1621.
71. Kornete M, Sgouroudis E, Piccirillo CA. ICOS-dependent homeostasis and function of $Foxp3^+$ regulatory T cells in islets of nonobese diabetic mice. *J Immunol*. 2012;188(3):1064–1074.
72. Farias FHG, et al. A rare regulatory variant in the MEF2D gene affects gene regulation and splicing and is associated with a SLE sub-phenotype in Swedish cohorts. *Eur J Hum Genet*. 2019;27(3):432–441.
73. Farh KK, et al. Genetic and epigenetic fine mapping of causal autoimmune disease variants. *Nature*. 2015;518(7539):337–343.
74. Yuan Z, Peng L, Radhakrishnan R, Seto E. Histone deacetylase 9 (HDAC9) regulates the functions of the ATDC (TRIM29) protein. *J Biol Chem*. 2010;285(50):39329–39338.
75. Kalin JH, et al. Targeting the CoREST complex with dual histone deacetylase and demethylase inhibitors. *Nat Commun*. 2018;9(1):53.
76. Boyman O, Kovar M, Rubinstein MP, Surh CD, Sprent J. Selective stimulation of T cell subsets with antibody-cytokine immune complexes. *Science*. 2006;311(5769):1924–1927.
77. Wang L, et al. $FOXP3^+$ regulatory T cell development and function require histone/protein deacetylase 3. *J Clin Invest*. 2015;125(8):3304.
78. Subramanian A, et al. Gene set enrichment analysis: a knowledge-based approach for interpreting genome-wide expression profiles. *Proc Natl Acad Sci U S A*. 2005;102(43):15545–15550.
79. Lin KY, et al. Treatment of established tumors with a novel vaccine that enhances major histocompatibility class II presentation of tumor antigen. *Cancer Res*. 1996;56(1):21–26.
80. Jackaman C, et al. IL-2 intratumoral immunotherapy enhances $CD8^+$ T cells that mediate destruction of tumor cells and tumor-associated vasculature: a novel mechanism for IL-2. *J Immunol*. 2003;171(10):5051–5063.
81. Lacoste B, Raymond VA, Cassim S, Lapierre P, Bilodeau M. Highly tumorigenic hepatocellular carcinoma cell line with cancer stem cell-like properties. *PLoS One*. 2017;12(2):e0171215.
82. Niedzielska M, et al. Differential gene expression in human tissue resident regulatory T cells from lung, colon, and blood. *Oncotarget*. 2018;9(90):36166–36184.